

A Sensorless PM Synchronous Motor Drive with Full Range Speed and Position Control using Feed Forward Torque Control

Greg Hunter, University of Technology, Sydney

Table of Contents

Nomenclature.....	2
I. Introduction.....	3
II. Structure of Feed Forward Torque Control for The Permanent Magnet Synchronous Motor.....	5
III. Detailed Description and Analysis.....	7
Feed-Forward Current to Voltage Conversion.....	7
Pulse Width Modulation.....	11
Load Model.....	12
Stabilisation at High Speed.....	13
Stabilisation at Low Speed.....	17
Torque Disturbance Correction.....	21
Direct Axis Current Setting.....	26
PWM Dead-Time Correction.....	26
Parameter Setting and Adaptive Parameter Adjustment.....	27
Motor Impedance Compensation.....	28
Sampling Delay Compensation.....	30
Speed Loop Implementation.....	33
Position Loop Implementation.....	35
IV. Simulation and Tuning.....	37
Servo Drive Simulation.....	37
Parameter Sensitivity of Servo Drive.....	44
Washer Direct Drive Simulation.....	47
Parameter Sensitivity of Washer Direct Drive.....	50
Difficult Loads.....	53
V. Experimental Verification.....	56
System Description.....	56
Equipment Used.....	57
Motor:.....	57
Load:.....	57
Inverter:.....	57
Controller:.....	58
Controller Settings.....	58
Performance Tests.....	58
Step Speed Response at Zero Speed.....	59
Step Speed Reversal.....	60
Step Load Response.....	60
Overload Response.....	60
References.....	61

Nomenclature

$*$, $'$, \sim	Superscripts indicating command value, applied value, estimated value
p	Differential operator
T	Motor electrical torque
T_L	Load torque
θ	Rotor angle, anticlockwise between rotor d axis and stationary α winding axis
λ_r	Rotor flux linkage (amplitude of fundamental component)
ω	Rotor speed in radians per second
R	Stator phase resistance
L	Stator phase inductance
J	Motor plus load inertia
ω_n	Natural resonant (hunting) frequency of the motor and load at high speed $= \lambda_r / \sqrt{LJ}$
R_n	Natural impedance of the motor and load $= \lambda_r \sqrt{L/J}$
i_d	d axis component of motor current
Δi_d	$i_d - i_d'$: d axis component of motor current error
i_q	q axis component of motor current
Δi_q	$i_q - i_q'$: q axis component of motor current error
i_q	q axis component of motor current
v_α	α phase motor voltage for two phase motor
v_β	β phase motor voltage for two phase motor
v_u	u phase motor voltage for three phase motor
v_v	v phase motor voltage for three phase motor
v_w	w phase motor voltage for three phase motor
V_{DC}	Inverter DC bus voltage
R_T	Total effective series q axis resistance at low speed
T_M	Load torque limit
i_{d0}	d axis component of motor current at zero speed
K_H	High speed stability compensation gain constant
ω_H	Filter roll off frequency in stability control path
K_1	Torque disturbance compensator 1 st order gain constant
K_2	Torque disturbance compensator 2 nd order gain constant
K_3	Torque disturbance compensator 2 nd order DC gain constant
$K_{\omega I}$	Speed feedback controller integral gain

- $K_{\omega p}$ Speed feedback controller proportional gain
- $K_{\omega f}$ Speed feedback controller natural frequency normalised to ω_n
- $K_{\omega d}$ Speed feedback controller damping factor
- R_I Added inverter generated output resistance
- L_N Added inverter generated negative inductance
- K_c Gain for voltage feedback correction loop
- τ_s Digital signal processor sample time synchronised to the PWM carrier.

I. Introduction

For fast dynamic control of electric motors, the drive control scheme normally has a fast inner torque or current controller surrounded by feedback speed and position controllers as required for the application.

The inner torque controller is normally a feedback type. The motor torque or torque generating current is measured directly or indirectly then compared with a reference torque or current, the error from which is then used to control the components of the applied motor voltage responsible for generating torque. Also required is a flux controller, which may be feedback or feed forward. This control structure has been very successful and has been almost universally used in both DC and AC motor drives.

A general block diagram of this type of controller for an AC motor is shown in Fig. 1. A feature of this type of controller is the need to measure or estimate the rotor position. This is used to calculate the angle of the motor flux which is needed to rotate the output voltage vector and the feedback current vector in synchronism with the flux. For a synchronous motor with a rotor angle sensor, the flux angle is just the rotor angle times the number of pole pairs. For an induction motor, the flux angle is usually indirectly determined from the measured rotor speed and an estimate of the slip frequency. For sensorless control of the motor, the flux angle must be estimated from the motor voltages and currents.

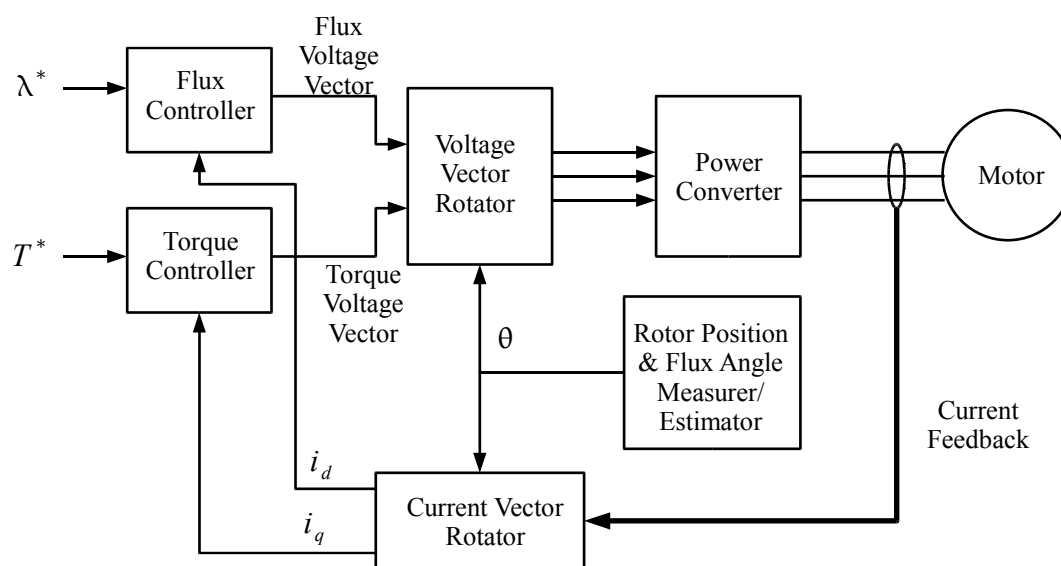


Fig. 1: Conventional torque controller.

A variation on this type of controller is the direct torque control method [1]. In this method, the motor torque and flux are calculated directly from the measured motor currents and the estimate of flux position without the need of a current vector rotator. The torque and flux controllers then use these direct values rather than the i_d and i_q currents. Also, the torque and flux controllers are hysteresis controllers directly determining the voltage vectors applied to the motor without using pulse width modulation (PWM).

When using a conventional torque controller with a permanent magnet synchronous motor (PMSM), estimating the rotor position without a rotor position sensor has proved particularly difficult. No universal method which will work with all PMSM types at all speeds has yet been devised. A summary of the various methods that have been devised so far are as follows.

For a permanent magnet motor with rotor saliency, such as an interior permanent magnet motor, it is possible to determine the rotor angle by directly measuring the spatial inductance variation by injecting a high frequency or pulse test currents [2]. One such system which has had some commercial success is the INFORM method [3,4]. The most advanced of such methods to date is the ellipsoid pattern high frequency injection method [5]. This method gains its high performance by directly measuring the spatial angular rate of change of inductance.

For permanent magnet motors without saliency, the only available method of determining the rotor angle is by using an estimation method using the motor's back-EMF. Many different estimators of this type have been devised [2]. The problem with these methods is that the back-EMF is too small at very low motor speeds to be measured and does not exist at all at zero speed. As a result, a back-EMF sensing method can only be used in applications where operation at zero and low motor speeds is not required. In such applications, the motor is usually started by injecting a current vector into the windings then spatially rotating the phase of the vector to drag the rotor around. Once enough speed is obtained, the controller switches to back-EMF sensing mode.

In this paper, rather than trying to solve the position estimation problem inherent in conventional torque controllers, a completely new torque controller structure is introduced which does not require knowledge of the rotor position to operate. This structure is designed to take advantage of the fact that the rotor position is controllable at zero speed, although not observable, to allow full speed range sensorless control. This new structure is called feed forward torque control (FFTC). A block diagram of FFTC is shown in Fig. 2. In this new structure, the torque voltage is calculated directly from the torque command in a feed-forward controller using estimates of the motor parameters and the motor flux. The applied rotor speed, from which the applied flux angle is calculated, is also found from the torque command using a model of the load. For synchronous machines, the applied flux angle is just the integral of the applied rotor speed, but for induction motors a correction must be added for the rotor slip. The load model is corrected for errors and unknown disturbances by feed-back of the torque producing current and comparing this with the expected current calculated from the command torque. In this way, any error in the flux angle will automatically cause a restoring torque to bring the error to zero. This scheme results in torque errors being corrected by changing the rate of acceleration rather than by changing the motor voltages as would occur in a traditional torque feed-back scheme. To prevent rotor speed oscillations (rotor hunting) due to the interaction of the restoring torque with the rotor inertia, some form of stability control should also be added to the load model.

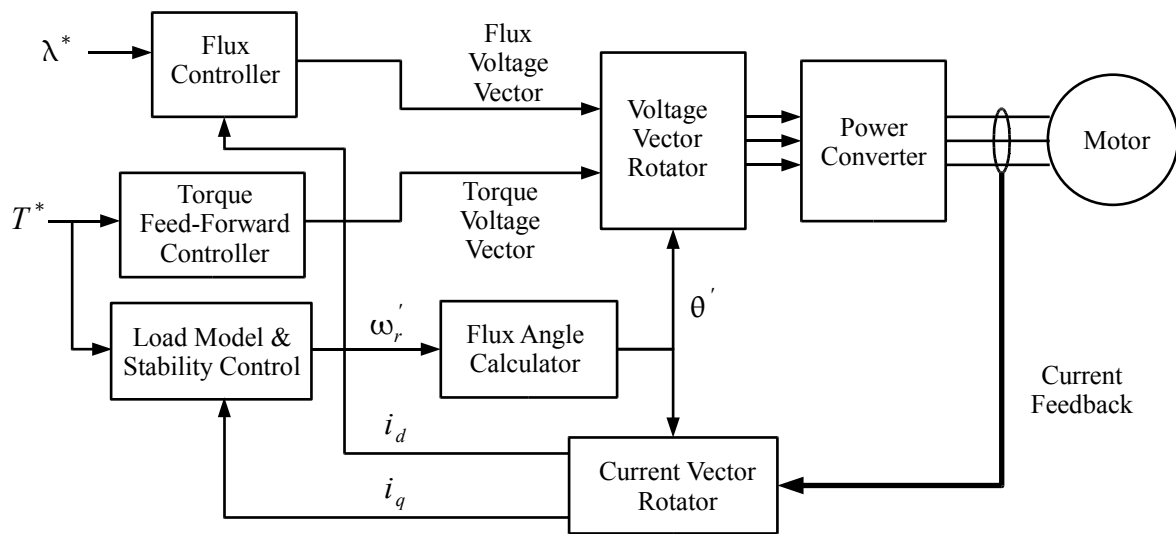


Fig. 2: The new feed-forward torque controller.

Using the new torque control structure allows fast dynamic control of the motor at all speeds. In addition, the slow response time to a change in the command torque introduced with a conventional feed-back torque control loop, especially with sampled data DSP control hardware, is removed. The response time for the change in motor torque to a change in the command torque is usually only one sample period.

An important feature of this new structure is that close approximations of the rotor speed and position are automatically made available at all speeds for use by the outer feedback loops. As well, the new structure places much lower demands on the hardware, with the required bandwidth of the current feedback signals being typically less than 100 Hz. This is a consequence of the feed-back current being used to control the load model which only involves mechanical time constants, rather than the electrical time constants associated with the conventional feed-back torque controller.

This paper presents the detailed implementation of FFTC for the non-salient synchronous permanent magnet motor. The structure of the control system as applied to this type of motor is presented in Section II, a detailed description and analysis is presented in Section III, simulation results are presented in Section IV, and experimental results are presented in Section V.

II. Structure of Feed Forward Torque Control for The Permanent Magnet Synchronous Motor

A feed forward torque control structure suitable for driving a non-salient PMSM is shown in Fig. 3.

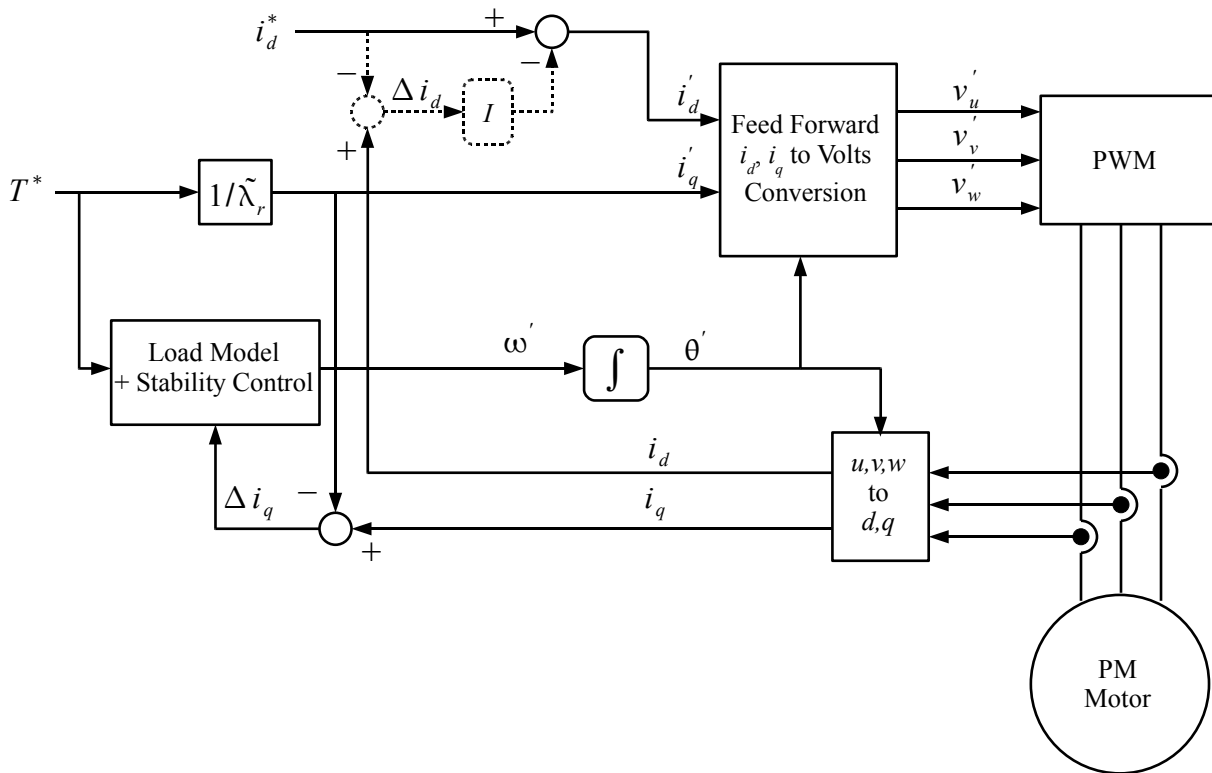


Fig. 3: Structure of feed forward torque control.

In this arrangement, the torque feed-forward controller, the flux controller and the voltage vector rotator of Fig. 2 are combined into the feed-forward i_d, i_q to volts conversion block. Combining these functions into the one block was found to greatly simplified the required algorithms. The flux is fixed by the rotor permanent magnets, so the flux command is replaced with the direct axis current command. Also, the torque command value is converted to the applied quadrature axis current i_d' by dividing it by the estimate of the rotor flux linkage. The error in the torque producing current Δi_q is used to correct the load model for unpredicted load disturbances and for correcting errors between the applied rotor position θ' and the actual rotor position θ .

Note that the dq axes referred to is actually the applied dq axes and not the true dq axes of the motor's rotor. When the controller is operating correctly the angle error between the two is minimised.

The accuracy of the d axis current can be improved by using feedback as shown dotted in Fig. 3. to modify the applied d axis current i_d' before the feed forward block. This is particularly useful at zero or near zero speeds when it is very difficult to precisely set the output current using open loop feed forward control only, especially for a motor with very low winding resistance.

Instead of estimating the rotor speed and position from either the back-EMF or high frequency injection, as in a conventional inner torque control structure for a sensorless PM motor, a model of the load is used to determine an applied rotor frequency ω' which is then integrated to obtain an applied rotor position θ' . To improve the load model, the difference between the applied q axis torque producing component of current i_q' and the measured value of this current i_q may be used to correct the load model. Usually the load model used just models the load inertia with the q axis current error being used to correct for added load torque.

The feed forward torque control method relies on the actual rotor position θ tracking the applied

rotor position θ' . For the permanent magnet synchronous motor, at high rotor speeds above the natural hunting frequency of the rotor and load, this occurs naturally. An increase in the rotor position error causes a change in the motor q axis component of current i_q resulting in the generation of an automatic restoring torque to correct the error. Without any modifications, though, the rotor damping of the oscillations caused by the interaction of the restoring torque and the rotor inertia is very poor. This instability can be successfully damped using a method proposed in [6] and later improved in [7]. This involves modulating the applied rotor frequency ω' with the deviation in the q axis component of current caused by the instability. A refined version of this method suitable for feed forward torque control of the permanent magnet synchronous motor described in a later section of this paper.

At very low speeds, the natural restoring torque which is a consequence of the back-EMF is too weak to lock the rotor position to the applied rotor position. Instead, at low speed, a different mechanism can be used. At these speeds, a positive value of the direct axis motor current i_d can be applied to lock the rotor into its correct position from the interaction of the rotor magnetic field and the field generated by this current. This is the mechanism by which stepping motors work, and as with stepping motors, good low speed position control can be achieved [8]. Unlike a stepping motor and controller, though, the direct axis motor current only needs to be high enough to correct the difference between the estimated load torque in the load model and the actual load torque. For a typical stepper motor controller, the direct axis current must be high enough to correct for all the expected motor torque including the usually dominant component, the inertial acceleration torque.

III. Detailed Description and Analysis

Feed-Forward Current to Voltage Conversion

The feed-forward conversion block generates the motor voltages required for the motor currents to track the input applied dq axes currents i_d' and i_q' for an input applied rotor angle θ' . The outputs of this block are the two-phase applied output motor voltages v_α' and v_β' which can then be converted to 3-phase output voltages for use by the PWM generator. The outputs of this block are generated using the motor equations linking v_α' and v_β' to i_d' and i_q' which are derived as follows:

Using the stationary $\alpha\beta$ axes shown in Fig. 4, the motor currents and voltages are related by the equation:

$$\begin{bmatrix} v_\alpha \\ v_\beta \end{bmatrix} = \begin{bmatrix} R i_\alpha \\ R i_\beta \end{bmatrix} + p \begin{bmatrix} L i_\alpha + \lambda_{r\alpha} \\ L i_\beta + \lambda_{r\beta} \end{bmatrix} \quad (1)$$

Converting the stationary $\alpha\beta$ frame currents and flux linkages to the rotating dq frame shown in Fig. 4 using the relationship:

$$\begin{bmatrix} \alpha \\ \beta \end{bmatrix} = \begin{bmatrix} \cos \theta & -\sin \theta \\ \sin \theta & \cos \theta \end{bmatrix} \begin{bmatrix} d \\ q \end{bmatrix} \quad (2)$$

and assuming the rotor flux is aligned on the d axis, giving $\lambda_{rd} = \lambda_r$ and $\lambda_{rq} = 0$, the following equation is obtained:

$$\begin{bmatrix} v_\alpha \\ v_\beta \end{bmatrix} = \begin{bmatrix} \cos \theta & -\sin \theta \\ \sin \theta & \cos \theta \end{bmatrix} \begin{bmatrix} R i_d \\ R i_q \end{bmatrix} + p \begin{bmatrix} \cos \theta & -\sin \theta \\ \sin \theta & \cos \theta \end{bmatrix} \begin{bmatrix} L i_d + \lambda_r \\ L i_q \end{bmatrix} \quad (3)$$

This equation can be expanded further to the following familiar motor voltage equations in the dq frame:

$$\begin{bmatrix} v_d \\ v_q \end{bmatrix} = \begin{bmatrix} R+Lp & -\omega L \\ \omega L & R+Lp \end{bmatrix} \begin{bmatrix} i_d \\ i_q \end{bmatrix} + \omega \lambda_r \begin{bmatrix} 0 \\ 1 \end{bmatrix} \tag{4}$$

where:

$$\begin{bmatrix} v_\alpha \\ v_\beta \end{bmatrix} = \begin{bmatrix} \cos \theta & -\sin \theta \\ \sin \theta & \cos \theta \end{bmatrix} \begin{bmatrix} v_d \\ v_q \end{bmatrix} \tag{5}$$

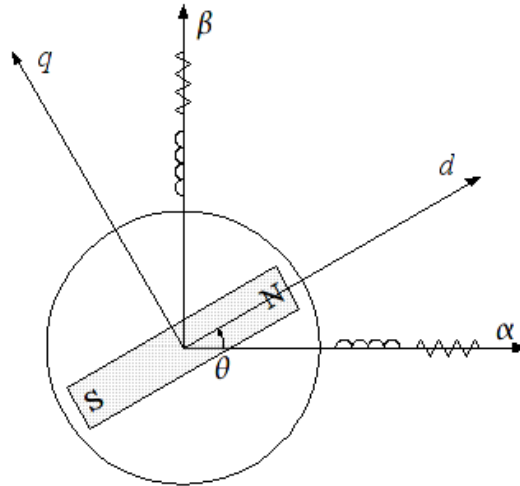


Fig. 4: Diagram showing the fixed and rotating axes representations of the two-phase PMSM.

In a conventional motor controller, a good example of which is described in [9], all calculations are implemented in the dq frame with the resulting dq frame motor voltages rotated to the $\alpha\beta$ frame for the PWM output. For the feed-forward current to voltage conversion block, it is possible to use the same procedure, first using equation (4) to generate the applied motor voltages in the dq axis then using equation (5) to convert to the $\alpha\beta$ frame.

An alternative and novel approach proposed here is to use the combined motor equation (3) directly. Some useful benefits are obtained using this approach. A block diagram of a suitable DSP implementation of the feed-forward block using equation (3) is shown in Fig. 5.

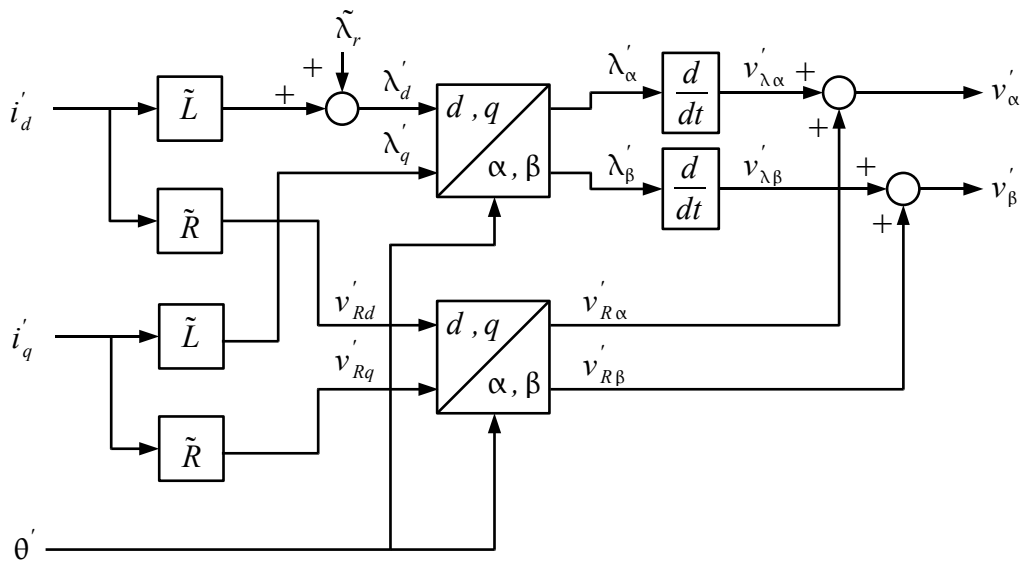


Fig. 5: Basic implementation of the feed-forward block.

For a DSP implementation, the DSP sample period for calculations is normally half the inverter PWM carrier period with each sample time synchronised to the start of a carrier half period. Sample periods which are multiples of a carrier half period can also be used. The dq to $\alpha\beta$ conversion block is usually implemented using sine and cosine look-up tables. When there are multiple reference frame rotation blocks, as is the case here, the sine and cosine of the applied angle need only be calculated once, then reused in each block. Each differentiation block in Fig. 5 can be implemented by subtracting the previous sample value from the new sample value at each sample, with multiplication by the inverse of the sample period T_s . This is shown in block diagram form in Fig. 6.

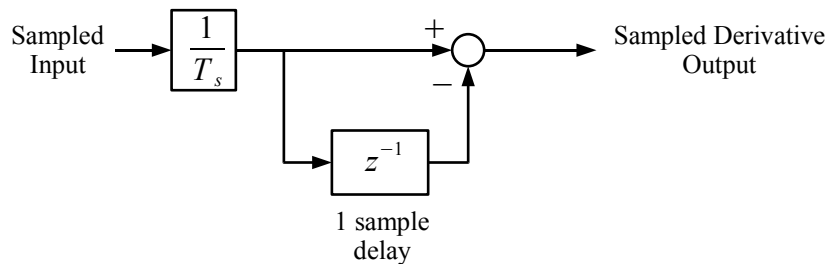


Fig. 6: Implementation of a differentiation block.

An advantage of using a direct implementation of equation (3) is that the sine and cosine look-up tables for the d, q to α, β conversion block do not need to be very accurate because an error in one sample value will cause a short term proportional current error only ($L \Delta i = \Delta \lambda$) which would be considerably less than the carrier induced current ripple anyway. Contrast this to a scheme using equations (4) and (5) where the vector rotation acts on the voltages instead of the flux linkages. The sine and cosine look-up tables now need to be very accurate because an error in one sample value causes a permanent step change in current ($L \Delta i = \int \Delta v dt$). Also in the feed-forward implementation scheme of Fig. 5 is the direct voltage to voltage vector rotation of the estimated motor IR drop voltages. Since these added voltages compensate only for the motor resistance voltage drops, the look-up tables for the dq to $\alpha\beta$ conversion also do not need to be very accurate.

Another advantage of using the direct implementation is that because the output voltages v'_{α} and v'_{β} are the change in flux linkage over each PWM carrier period or half period, these voltages are equal to the average expected voltages over this period ($\Delta \lambda = \Delta \int v dt$). The resulting PWM pulse widths are thus proportional to the average output voltages over that period. It has been shown [10] that this greatly reduces subharmonic currents when the carrier to output frequency ratio is low.

For large changes between successive sampled values of the applied flux linkages λ'_{α} and λ'_{β} caused, for instance, by a step change in the torque command, the output sampled value of each differentiation block could be large enough to cause clipping in the PWM output voltage. This would result in the needed change in flux linkage and the corresponding change in current not appearing on the motor. To prevent this happening, an extra pulse lengthening block can be added after differentiation to limit the peak voltage without changing the voltage integral. Because the output voltage also includes the IR voltage drop compensation component added after differentiation, the pulse lengthening process must also take this extra voltage into account. A suitable method of implementing the required pulse lengthening is shown in Fig. 7. This pulse lengthening and clipping unit modifies the applied output stationary axis voltages v'_{α} and v'_{β} by clipping their vector magnitude and adding the resultant errors to the inputs at the next sample.

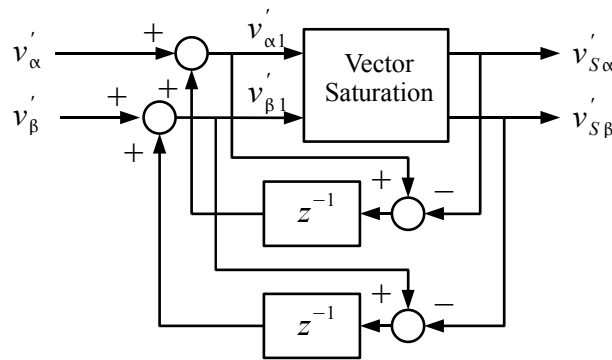


Fig. 7: Method of pulse clipping and lengthening.

This method of pulse lengthening is only approximate. It assumes the change in the applied IR drop voltages $v'_{R\alpha}$ and $v'_{R\beta}$ and the change in the applied flux angle θ' are not significant during pulse lengthening. A more complex pulse lengthening method may be needed for a motor with high inductance or high winding resistance, or for a low output frequency to sample frequency ratio.

The vector saturation unit clips the v'_{α}, v'_{β} vector to a fixed magnitude so it is limited to a circle in the space vector plane. For maximum utilisation of the available inverter output voltages, assuming a six switch 3 phase inverter is used, clipping to a hexagon limit can be implemented. The two limits on the space vector plane are shown in Fig. 8.

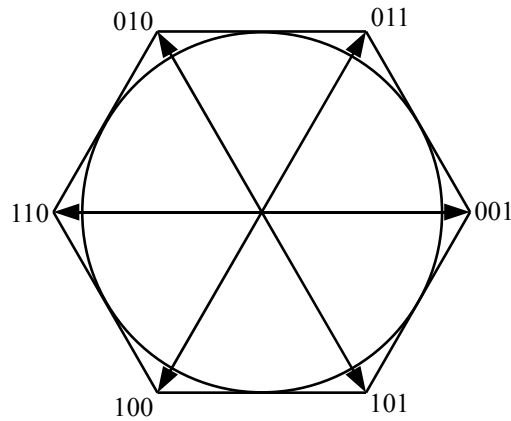


Fig. 8: Inverter output space vectors showing hexagonal limit and proposed circular limit.

A simple method of implementing clipping to a circle which avoids calculating the vector angle is shown in Fig. 9. The vector components are normalised by dividing by the vector magnitude then rescaled using the clipped value of the magnitude. To reduce the computational load, the vector magnitude need not be calculated accurately.

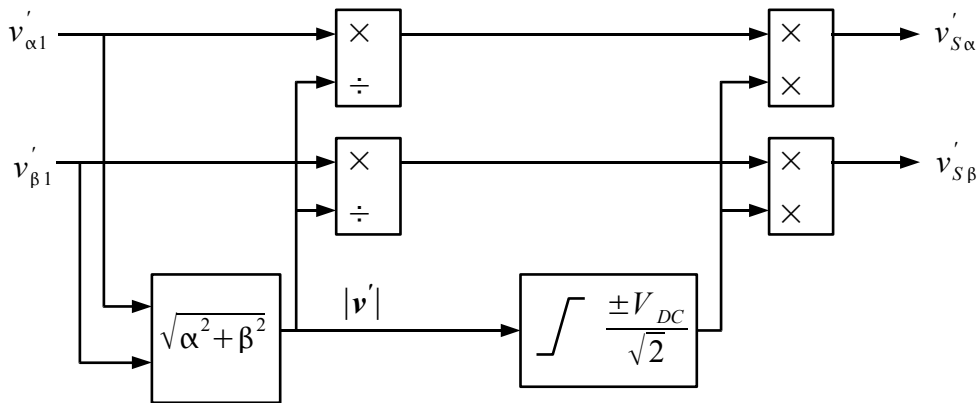


Fig. 9: Vector saturation of the applied phase voltages.

An alternative method of effective pulse lengthening is to limit the rate of change of the vector magnitude of the total flux linkage. This could be implemented either before or after the vector rotation from the dq to the $\alpha\beta$ reference frames in Fig. 5.

Pulse Width Modulation

The two most common methods of generating the actual output pulse width modulated output voltages from the output voltage signals are space vector modulation and triangle carrier-based modulation. It is difficult to apply space vector modulation to FFTC because the angle of the applied output voltage signal vector is not known and can be difficult to calculate from the vector components $v_{S\alpha}'$ and $v_{S\beta}'$. Instead, carrier-base modulation will be used. As shown in [11], with proper application, there is little difference between the performance of the two methods.

The PWM process used in the experimental set-up as implemented on a dSpace hardware system is shown in Fig. 11. The stationary frame output voltage signals $v_{S\alpha}'$ and $v_{S\beta}'$ are first converted to

three phase format and then centred within the DC bus limits before feeding to the pulse width modulators.

The two to three-phase conversion of the output voltage signals uses the power preserving conversion formula of equation (6).

$$\begin{bmatrix} v'_u \\ v'_v \\ v'_w \end{bmatrix} = \sqrt{\frac{2}{3}} \begin{bmatrix} 1 & 0 \\ -\frac{1}{2} & \frac{\sqrt{3}}{2} \\ -\frac{1}{2} & -\frac{\sqrt{3}}{2} \end{bmatrix} \begin{bmatrix} v'_{S\alpha} \\ v'_{S\beta} \end{bmatrix} \tag{6}$$

For clarity, the relation between the u, v, w and the α, β vectors is shown graphically in Fig 10.

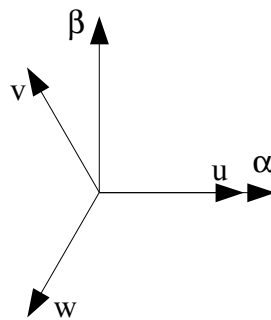


Fig. 10: Vector diagram showing the relation between the u, v, w and the α, β vectors.

The centring of the three phase applied output voltages is equivalent to having equal start and finish null vector times in the space vector modulation method. The output voltage signals v'_u, v'_v and v'_w can, after suitable scaling with the inverse of the measured inverter DC bus voltage and offset adjustment, be sent to a hardware carrier-based PWM generator as found in most motor control DSP's.

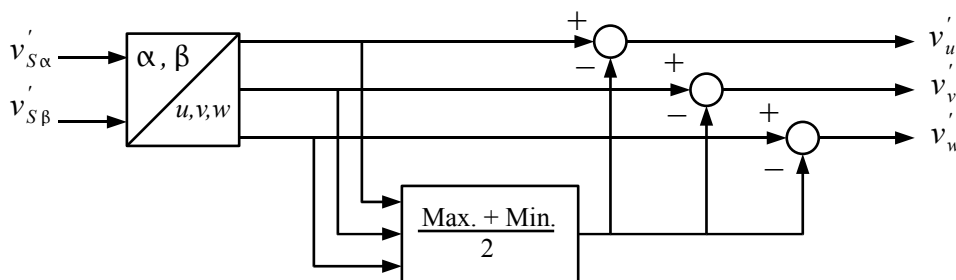


Fig. 11: Method of centring the PWM inputs.

Although not implemented here, it is often advantageous to clamp the PWM output voltages to alternatively the positive and negative DC bus limits as described in [12] instead of centring them to minimise switching losses.

Load Model

As shown in Fig. 3, a load model is required to find the applied motor speed ω' from the reference torque. For most applications, a basic inertial model is sufficient. This model assumes the following relationship between the torque and speed, shown Laplace transformed :

$$\omega = \frac{T}{J_s} \tag{7}$$

This equation is implemented as the load model by using an estimate of the total inertia. The load model block implementing this equation is shown in Fig. 12.

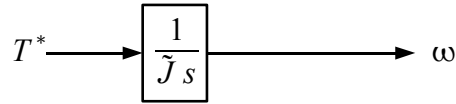


Fig. 12: Load model block for an inertia load.

As will be shown later, at high speeds, errors caused by added load torque can be corrected using the measured rotor flux oriented q axis component of motor current. At low and zero speed, any added load torque will cause an error in the rotor angle which can be constrained by setting a high d axis component of motor current.

If more information about the load is known, this can be added to the load model for improved performance. For instance, if the variation in load torque with speed is known then this can be added as shown in Fig. 13 where $f_T(\omega)$ is the function describing the load torque against speed.

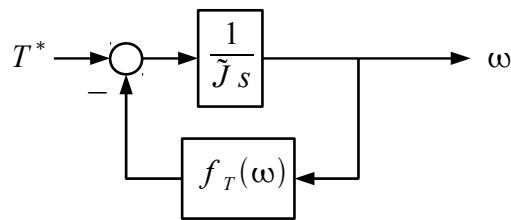


Fig. 13: Load model block with added load torque against speed function.

Stabilisation at High Speed

If the load model only was used to generate the applied rotor speed ω' , the motor would exhibit instability, with the actual motor speed oscillating about the applied speed. To prevent this, electrical damping must be added to the control structure. There are two modes of oscillation, one that occurs at high speed and another that occurs at low and zero speed and each mode requires a different damping procedure. In this section, the mode of oscillation at high speed is analysed and a method of damping it is proposed. The low speed oscillating mode is examined in the next section.

The oscillation in rotor speed of the PMSM when operating with a fixed frequency at high speed is well known. An exact analysis of the phenomenon is given in [7]. Here, a simplified analysis similar to that presented in [6] is given. This analysis is sufficient for choosing the parameters in a controller design.

Consider the case of a two pole PMSM operating without load at a high fixed stator frequency ω and with the rotor emf vector, E , equal to the applied voltage vector, V . Now consider the case of a small perturbation of δ radians in the rotor angle due to instability causing a current I to flow. At high speed, the motor reactance ωL , is much larger than the motor resistance and the phasor diagram shown in Figure 14 applies.

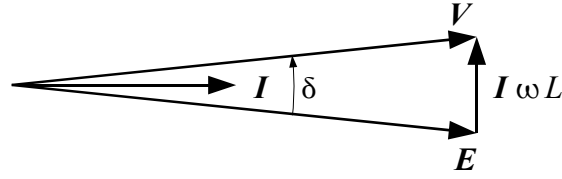


Fig. 14: Phasor diagram for rotor retarded by angle δ .

Assuming δ is very small, with the applied q axis aligned with the voltage vector V and with E equal to $\lambda_r \omega$, then $I \simeq i_q$ and the resulting q axis current is given by:

$$i_q = \frac{\lambda_r \delta}{L} \quad (8)$$

The resulting restoring torque, T , is given by:

$$\begin{aligned} T &= \lambda_r i_q \\ &= \frac{\lambda_r^2 \delta}{L} \end{aligned} \quad (9)$$

Coupled with the motor inertia J , the resultant simple harmonic motion is described by the differential equation:

$$J \frac{d^2 \delta}{dt^2} = -\frac{\lambda_r^2}{L} \delta \quad (10)$$

Replacing δ with T as the independent variable using equation (9):

$$J \frac{d^2 T}{dt^2} = -\frac{\lambda_r^2}{L} T \quad (11)$$

In reality, there will be a steady state torque and q axis current as well as the oscillating torque and current so torque T in the above equation should be replaced with the change in torque ΔT , giving the differential equation describing the oscillation as:

$$J \frac{d^2 \Delta T}{dt^2} = -\frac{\lambda_r^2}{L} \Delta T \quad (12)$$

By comparing this to the equation for an LC tuned circuit with :

$$C_M \frac{d^2 i(t)}{dt^2} = -\frac{1}{L_M} i(t) \quad (13)$$

where L_M and C_M are the mechanical equivalent inductance and capacitance values, the quasi steady state differential equation (12) can be conveniently represented by the LC equivalent circuit of Fig. 15. This tuned circuit analogy is an excellent way of viewing the main system energy storage states involved in the oscillation which are not readily apparent in a mathematical representation. It is an alternative method of stability analysis which will be used extensively in this paper. It is particularly useful at handling high order systems.

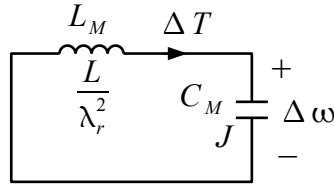


Fig. 15: High speed quasi-steady-state mechanical equivalent circuit.

The capacitor in Fig. 15 represents the load inertia. The voltage across it, as shown, gives the quasi steady state change in rotor speed $\Delta \omega$ during the oscillation.

The resonant frequency of this system, which is called the natural frequency ω_n , is an important parameter in the design of the controller. Its value is given by the equation:

$$\omega_n = \frac{\lambda_r}{\sqrt{LJ}} \quad (14)$$

To apply damping to the above resonant system, a series equivalent resistance can be inserted in the equivalent tuned circuit. To do this, first a forcing function is added in series in the circuit by adding a modulation $\Delta \omega'$ to the applied frequency from the inverter. This appears in the equivalent tuned circuit as an equivalent forcing voltage as shown in Fig. 16. Note that with the feed forward block as implemented in Fig. 5, when a change in frequency is made, a change in the q axis output voltage of magnitude $\lambda_r \Delta \omega'$ also occurs. At high speed, where the back-EMF is much larger than this change in voltage, it has little effect on the q axis current. As will be seen later, at low speed, the reverse is true: the q axis current is affected mainly by this voltage change and not by the change in the applied frequency.

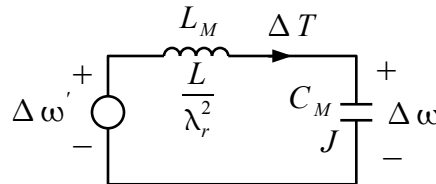


Fig. 16: High speed mechanical equivalent circuit with forcing function $\Delta \omega'$.

To provide damping, the forcing function $\Delta \omega'$ can be made proportional to the change in torque ΔT to create an equivalent series damping resistance. For a damping factor ζ , the equivalent series damping resistance is $2\zeta \sqrt{L_M/C_M}$ and the required forcing function is given by the equation:

$$\Delta \omega' = -\frac{2\zeta}{\lambda_r} \sqrt{\frac{L}{J}} \Delta T \quad (15)$$

In the actual controller, the measured parameter is i_q rather than torque, so changing ΔT to Δi_q as the independent variable, equation (15) becomes:

$$\Delta \omega' = -2\zeta \sqrt{\frac{L}{J}} \Delta i_q \quad (16)$$

The high speed damping can be incorporated into the load model block of Fig. 3. Combining the

simple inertia load model of equation (7) with high speed damping, the Laplace transform of the load block implementation is now:

$$\omega' = \frac{T^*}{\tilde{J}_s} - 2K_H \sqrt{\frac{\tilde{L}}{\tilde{J}}} \Delta i_q \tag{17}$$

where K_H is defined as the high speed damping constant and is equal to the damping factor ζ .

The resulting load model plus stability control block is shown in Fig. 17.

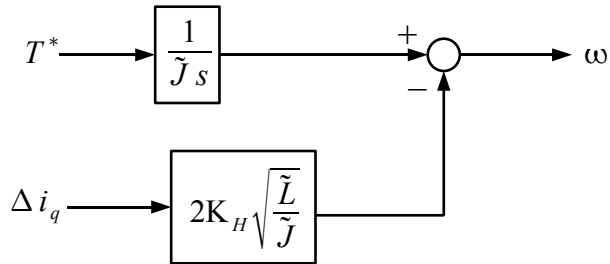


Fig. 17: Load model and stability control incorporating high speed damping.

The damping circuit of Fig. 16 with the series equivalent damping resistance added is shown in Fig. 18.

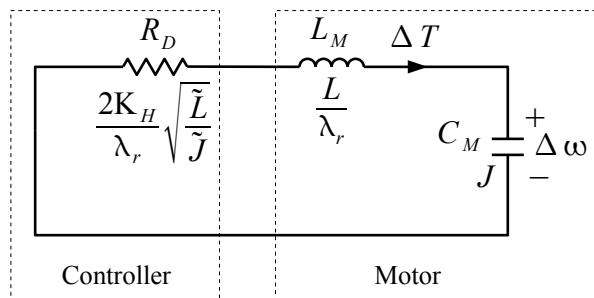


Fig. 18: High speed mechanical equivalent circuit for damping.

The effect of the command torque, T^* can be approximately represented by the circuit of Fig. 19. The torque command current source emulates the effect of the torque feed forward path and the integral of torque voltage source emulates its effect on the rotor speed via the load model. As can be seen, a change in the command torque does not excite the tuned circuit allowing command torque response times much faster than the motor's electrical time constants. Note that this is only true provided the motor parameters used in the controller match the actual motor parameters. Also shown shaded in Fig. 19 is the effect of a load torque disturbance, T_L . This does excite the tuned circuit and so the response to a disturbance depends on the tuned circuit resonant frequency and damping.

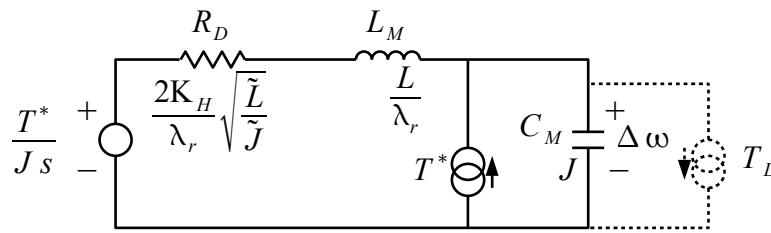


Fig. 19: Equivalent circuit showing the effect of the command torque and a load disturbance torque.

Stabilisation at Low Speed

At speeds much less than the natural frequency ω_n , the high speed restoring torque disappears and an alternative method must be used to hold the rotor angle θ in alignment with the applied rotor angle θ' .

Fortunately restoring torque can be applied at low speed by applying current in the d axis, turning the motor into a stepping motor. This restoring torque, like the restoring torque created at high speed, creates its own resonance from interacting with the motor inertia which must be damped. This damping problem is well known in the control of stepping motors. Usually mechanical damping is relied upon, but various electromagnetic damping methods have also been proposed [13,14].

To analyse the resonances and develop a method of damping, an electrical circuit analogy will again be used. Consider a two-phase, two-pole PMSM with no external load except the load inertia and with a quasi-stationary rotor with the d and q axes aligned with the two windings. Assume a fixed current in the winding aligned with the d axis locking the rotor to this axis. A simplified diagram of the motor with a quasi-stationary rotor showing the q axis winding is illustrated in Fig. 20. Now consider the equivalent electrical LC circuit for the stationary q axis for an undamped oscillating rotor with the q axis winding open circuit. The equivalent LC tuned circuit is shown in Fig. 21. The equivalent parallel inductance is L_p and the equivalent capacitance is C_p .

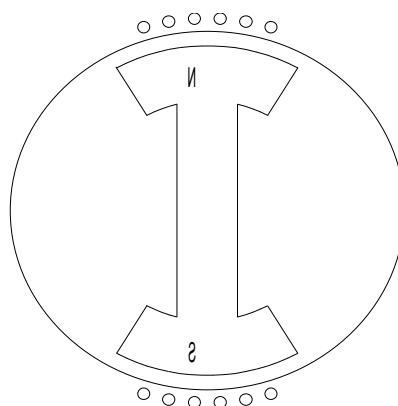


Fig. 20: Motor with a quasi-stationary rotor showing the q axis coil for analysis of rotor resonance

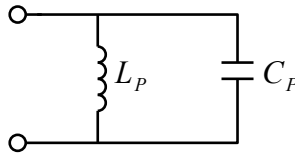


Fig. 21: Stationary open circuit q axis equivalent circuit with fixed d axis current.

Now consider the effect of the restoring torque generated by the fixed d axis current when the q axis winding is open circuit. When the rotor moves off the d axis by an angle δ , the resulting restoring torque is $i_d^* \lambda_r \sin \delta$ or $i_d^* \lambda_r \delta$ to a first approximation. The resulting equation of motion is:

$$J \frac{d^2 \delta}{dt^2} = -i_d^* \lambda_r \delta \tag{18}$$

For electrical circuit equivalence, this must match the differential equation for the tuned circuit which is:

$$C_p \frac{d^2 i(t)}{dt^2} = -\frac{1}{L_p} i(t) \tag{19}$$

The tuned circuit component values can be found by matching terminal voltage, energy and resonant frequency. The q axis terminal voltage $\lambda_r d \delta / dt$ is the voltage on the capacitor giving the energy stored in the capacitor as $0.5 C_p (\lambda_r d \delta / dt)^2$. This is the kinetic energy $0.5 J (d \delta / dt)^2$, giving:

$$C_p = \frac{J}{\lambda_r^2} \tag{20}$$

Matching the inverse square of the resonant frequencies gives $L_p C_p = J / (i_d \lambda_r)$ giving a value for the inductor of:

$$L_p = \frac{\lambda_r}{i_d} \tag{21}$$

Finally, equating the capacitor voltage $\lambda_r d \delta / dt$ to the inductor voltage $L_p di_p / dt$, where i_p is the inductor current, then integrating and assuming zero initial conditions, the rotor deviation angle is found to be:

$$\delta = \frac{i_p}{i_d} \tag{22}$$

The value for C_p of J / λ_r^2 is, not unexpectedly, the same as the capacitance in the high speed equivalent circuit of Fig. 16 with the variables changed from torque to current (using $i = \lambda_r / \Delta T$) and from rotational speed to voltage (using $v = \lambda_r \Delta \omega$).

To complete the q axis equivalent circuit for quasi-stationary rotor oscillations, the winding inductance and resistance can be added as shown in Fig. 22. This circuit model was derived for a stationary motor with no load but it also holds for low speed operation and a fixed torque load with added compensating q axis current.

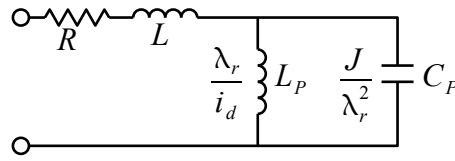


Fig. 22: Complete equivalent circuit of the motor at low speed.

It can be seen from this LC equivalent circuit that to provide damping at low speeds, the inverter can provide a resistive output impedance in the q axis but the level of damping will be limited if a high d axis current results in the equivalent inductance L_p being comparable with the motor winding inductance.

The d axis command current must be set at least high enough so that the pull-out torque, $\lambda_r i_d$, is higher than the maximum expected error between the actual and the load modelled torque. It may need to be set higher than this minimum value to reduce the maximum rotor angle error (for, example, better position control) or to reduce the settling time of the rotor on start up. If the d axis current is set too high, inductance L_p could be too low compared to the winding inductance to allow adequate low speed damping as can be seen in the equivalent circuit. As will be shown later in this paper, it is possible to improve damping in this situation by adding negative inductance to the inverter generated output impedance.

The added inverter generated resistance must be chosen so that this resistance plus the winding resistance provides adequate damping for both the series LC_p tuned circuit and the parallel $L_p C_p$ tuned circuit. For fastest rotor settling time at start up and after torque disturbances, the total series resistance R_T should be set for approximately critical damping of the parallel tuned circuit, i.e. $R_T = 0.5 \sqrt{L_p / C_p}$. For maximum robustness to torque disturbances, it should be set for approximately critical damping of the series tuned circuit, i.e. $R_T = 2 \sqrt{L / C_p}$. Usually a compromise between these settings is made.

If the controller high speed damping shown in Fig. 17 and equation (17) is left in place at low speeds, a change in applied speed $\Delta \omega'$ from a change in Δi_q automatically produces a corresponding change in the q axis terminal voltage of $\lambda_r \Delta \omega'$. From equation (16), the resulting inverter impedance $\lambda_r \Delta \omega' / \Delta i_q$ is given by:

$$\frac{\lambda_r \Delta \omega'}{\Delta i_q} = 2K_H R_n \quad (23)$$

where R_n is the natural impedance of the motor and is defined as $\lambda_r \sqrt{L/J}$.

Not surprisingly, this provides the correct resistance for damping the LC_p tuned circuit if the winding resistance is ignored. Often, this resistance plus the winding resistance is enough to provide adequate damping of the $L_p C_p$ tuned circuit but sometimes an extra inverter generated resistance is needed.

If an extra inverter resistance R_I on top of the inverter generated resistance from the high speed damping is added, the total effective winding resistance will be:

$$R_T = 2K_H R_n + R + R_I \quad (24)$$

The extra electronically generated resistance is best added by modifying the feed forward block in Fig. 5 to that shown in Fig. 23. To balance the output impedance in both the d and q axis, an extra electronic resistance of $2K_H \tilde{R}_n + R_I$ has also been added to the d axis. This ensures the rotor damping remains the same even for large deviations between the rotor and applied rotor angles

which may occur at start-up.

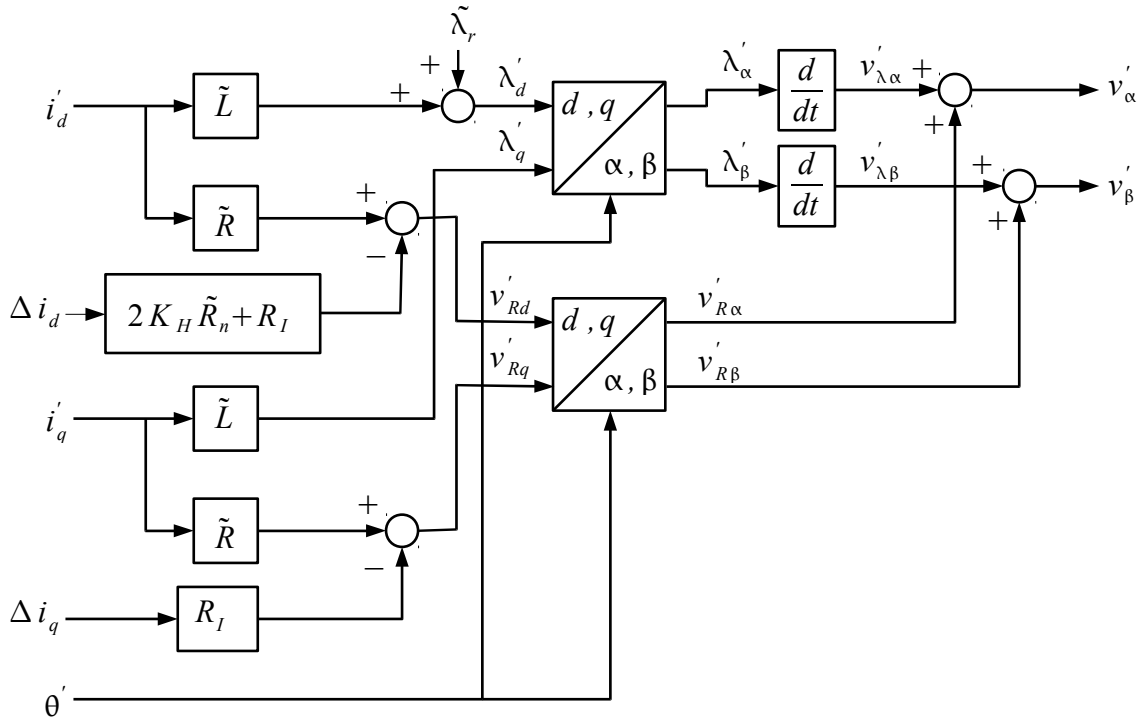


Fig. 23: Feed forward block with added rotor damping resistance.

If the winding resistance is very large, it may be necessary to make R_l negative in order to provide the required low speed damping. Also, if inductance L is too large to find a compromise effective damping resistance for both the LC_P and $L_P C_P$ tuned circuits, it may be necessary to modify the inverter output impedance to include a negative inductance. Adding electronically generated negative impedances to the inverter output must be implemented carefully. It usually requires higher current bandwidth and accurate compensation of PWM dead time. The topic is dealt with more fully further on in this paper.

It is of interest to note that as the applied frequency drops below the natural frequency the effect on damping of modulating the applied frequency rapidly diminishes. At zero Hz, with the applied voltage zero, it has no effect at all. Equally, as the applied frequency is raised above the natural frequency, the effect on damping of modulating the applied voltage also rapidly diminishes due to the diminishing ratio of the modulating voltage to the back-EMF. The two damping methods complement each other to provide the same level of damping throughout the speed range.

In this paper, the low frequency damping and high frequency damping are treated separately. It would be very beneficial to combine the high frequency mechanical equivalent circuit of Fig. 18 and the low frequency electrical equivalent tuned circuit of Fig. 22 into one, but there is no obvious way of doing this due to the complex impedance the motor presents to the inverter at high frequencies.

Torque Disturbance Correction

So far, the controller is designed to respond very quickly to changes in the command torque, but there is no provision for it to respond properly to a load torque disturbance. A load torque disturbance not incorporated into the load model will result in a corresponding rotor angle error. There will be a slight correction from the feedback of Δi_q used for stability control but this would be minor.

What is required is for a fixed command torque, when the load torque is changed, the applied acceleration must be changed until the inertia generated torque balances the change in load torque to make the electrical torque equal to the command torque. The required balance is shown in the following equation:

$$J \Delta \frac{d \omega'}{dt} = -\Delta T_L \tag{25}$$

At high rotor speeds, an error ΔT between the command torque and the electrical torque produces a q axis current error as follows:

$$\Delta T = \lambda_r \Delta i_q \tag{26}$$

The load model can be adjusted to add partial correction for a torque disturbance by adding integral feedback of the q axis current error to the applied frequency, extending the load model and stability control equation (17) to:

$$\omega' = \frac{1}{\tilde{J}_s} (T^* - K_1 \tilde{\lambda}_r \Delta i_q) - 2K_H \sqrt{\frac{\tilde{L}}{\tilde{J}}} \Delta i_q \tag{27}$$

where K_1 is the 1st order load compensation gain constant.

The corresponding block diagram of the load model and stability control block is shown in Fig. 24.

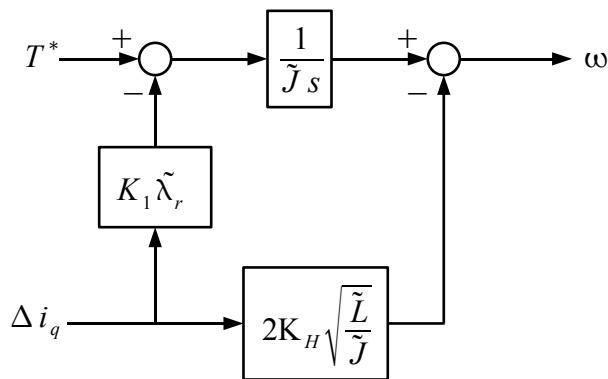


Fig. 24: Load model and stability control incorporating 1st order load torque correction.

At high rotor speeds, the effect of this modification when considering the quasi steady state mechanical equivalent damping circuit of Fig. 18 is to add a series capacitance as shown in Fig. 25 and at low speed, the effect on the q axes equivalent circuit is shown in Fig. 26.

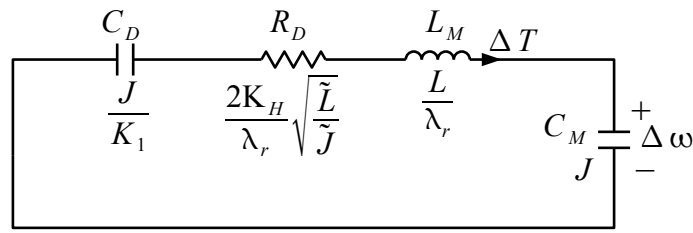


Fig. 25: Quasi steady state mechanical equivalent damping circuit at high speed with 1st order load correction.

The maximum value that can be set for K_1 is limited by its effect on rotor damping. Its value can be chosen by incorporating its effect in the low speed damping equivalent circuit of Fig. 22. The resulting equivalent circuit is shown in Fig. 26. In this circuit, the new 1st order term appears as a series capacitance C_1 of value $1/K_1$ times the inertia capacitance C_P .

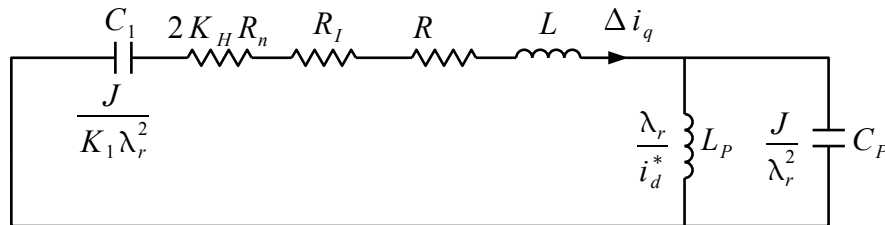


Fig. 26: Quasi steady state q axis equivalent damping circuit at low speed with 1st order load correction.

This circuit is fourth order making the choice of component values difficult. If motor inductance L is ignored, the circuit shows that to be able to choose a value of $R_T = 2K_H R_n + R + R_I$ to give approximately critical damping for both the $C_P L_P$ tuned circuit and the $C_1 L_P$ tuned circuits, R_T must satisfy the equations:

$$R_T = 0.5 \sqrt{\frac{L_P}{C_M}} \tag{28}$$

and:

$$R_T = 2 \sqrt{\frac{L_P}{C_1}} \tag{29}$$

This requires C_1 to be at least 16 times the value of C_P . Such a system would be very slow to respond to load torque transients, so usually a choice of C_1 much close to the value of C_P is better, with R_T chosen as:

$$R_T = \sqrt{\frac{L_P}{\sqrt{C_1 C_P}}} \tag{30}$$

If L is not much smaller than L_P , then R_T may need further adjustment to provide adequate damping of the $L C_1 C_P$ tuned circuit. Usually adjustment by simulation of the low speed damping circuit is required. In almost all applications, a value of C_1 of twice C_P , is the best compromise. This gives a setting for stability constant K_1 of 0.5.

Note that at high speeds, the equivalent circuit for stability analysis reverts to that of Fig. 25 and the effect of the parallel branch L_P disappears. This allows the series capacitance, in this case C_D , to

be much higher than the inertia equivalent capacitance C_M , with the corresponding value of K_1 set to much greater than 1. This lifts the effective natural resonant frequency greatly reducing response times. To implement this, K_1 would have to be made a function of frequency. This has not been investigated in this paper.

A side benefit of adding the above integral feedback control of the q axis current at low speeds is that errors in the feedback loop are compensated for. In particular, at very low speeds and at standstill, errors in the PWM process such as dead band voltage errors do not result in q axis current errors.

To add robustness to the controller against errors in the motor parameter settings and against torque disturbances at low speed which cannot be compensated for, it is advisable to introduce a matching integral controller in the d axis. This can be implemented as the dotted integral controller shown in Fig. 3. The required integral controller has the following s domain transfer function:

$$i'_d = i_d^* - \Delta i_d \frac{K_1 \omega_n}{s} \quad (31)$$

This is implemented as shown in Fig 27. As in the q axis integral feedback controller, this controller stabilises the output d axis current against errors. This is particularly important since even slight variations in the estimated rotor flux could otherwise cause large errors in the d axis current.

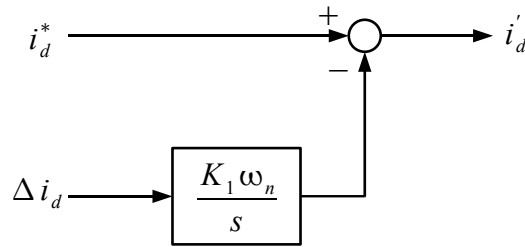


Fig. 27: d axis integral current compensator.

The first order torque disturbance compensation shown in Fig. 24 cannot properly correct for a step torque disturbance. Such a disturbance requires the motor to be accelerated at a constant rate after the change in load torque, resulting in a fixed torque offset error for a first order compensation system. This can be corrected by adding a second order term to the transfer function of equation (27). The new transfer function is then:

$$\omega' = \frac{1}{\tilde{J}s} \left(T^* - K_1 \tilde{\lambda}_r \left(1 + K_2 \frac{\omega_n}{s} \right) \Delta i_q \right) - 2K_H \sqrt{\frac{\tilde{L}}{\tilde{J}}} \Delta i_q \quad (32)$$

This can be implemented as shown in Fig. 28. The load torque correction ΔT_m which appears at the output of the second order integrator block is, at higher speeds, the error between the torque predicted by the load model and the actual torque. It is possible to use this value to adaptively correct the load model to improve dynamic performance. This will be considered later in this paper.

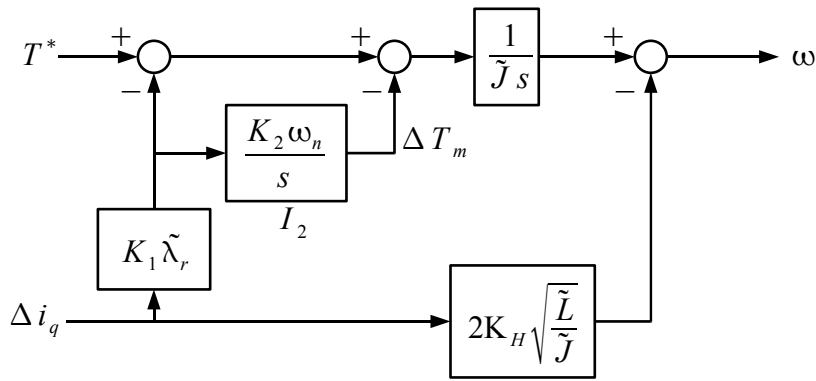


Fig. 28: Load model and stability control incorporating 2nd order load torque correction.

For the first order torque disturbance correction term, a matching compensator was added to the d axis current controller. A matching second order term is not needed though for the d axis controller and would be difficult to implement.

The second order term is difficult to incorporate into the high speed quasi steady state equivalent circuit damping model of Fig. 25 but at the circuit's resonance it injects a frequency modulation 180 degrees out of phase with the torque modulation, so its effect on damping can be compensated by slightly increasing the equivalent series damping resistance by increasing K_H . The same increase in K_H should also correct for the effects of the second order term on low speed damping.

This second order load disturbance feedback correction system creates an interesting dilemma at zero speed. Without a back EMF present, any load torque offset at low speed will not cause a change in the motor current. As a result, it is possible at zero speed for the system to be stable for any value of T^* with i_q adjusted to match it but with an unmatched true motor torque. The rotor true d axis will just align at a 90 degrees shift to the total current vector angle less a torque balance shift, with the true torque being unmeasurable. In the load model block, the system will be stable with $\Delta i_q = 0$ and ΔT_m equal to T^* . The output of the second order block is effectively what the control system thinks the load torque is.

To prevent this problem of multiple stable states at zero speed, a pole can be added to the integrator block I_2 in Fig 28 limiting its DC gain to force it to settle at zero output at zero speed. The pole is needed at zero speed but is not needed at high speed, so the DC gain should be modulated by a frequency dependent function to limit its effect at high speed. The simplest way to implement this is with a variable gain feedback path around the integrator as shown in Fig. 29. With the pole added, the transfer function for the load model and stability control block, equation (32), now becomes:

$$\omega' = \frac{1}{\tilde{J}s} \left(T^* - K_1 \tilde{\lambda}_r \left(1 + \frac{K_2 \omega_n}{s + K_2 \omega_n K_3 F_0(\omega_f')} \right) \Delta i_q \right) - 2K_H \sqrt{\frac{\tilde{L}}{\tilde{J}}} \Delta i_q \quad (33)$$

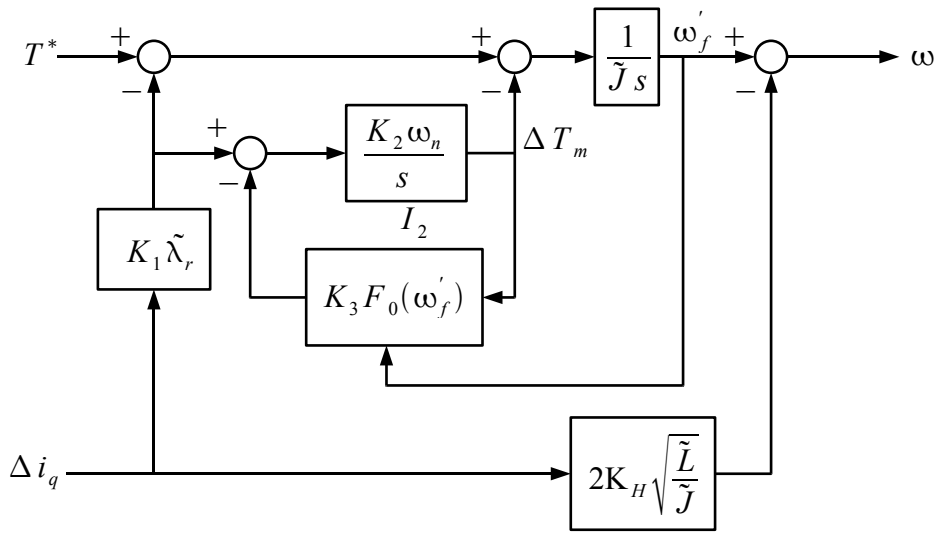


Fig. 29: Load model and stability control with a variable limit on the 2nd order DC gain.

The DC gain of integrator I_2 at zero speed is now $1/(K_3 F_0(\omega'_f))$ and thus is determined by the fixed gain constant K_3 and the gain function $F_0(\omega)$. A suitable formula for the function $F_0(\omega)$ is:

$$F_0(\omega) = \frac{\omega_n}{|\omega| + \omega_n} \tag{34}$$

This function gives a gradual increase in the DC gain with frequency with the gain doubled at the natural resonant frequency. Other functions may be better depending on the application. In the arrangement shown in Fig. 29 a filtered version ω'_f of the rotor applied frequency obtained before the stabilising term is added is used for the function's independent variable but ω' could also be used.

The setting of the DC gain constant K_3 depends on the application. If the load torque is expected to stay fixed as the motor goes through zero speed then K_3 can be set to a very low value ($\ll 1$). The control system will then retain the correct value of i'_q as the motor goes through zero speed. In effect, the controller 'remembers' the load torque applied before zero speed is reached. A practical example where this control setting would be advantageous is a direct drive washer motor [15] which, during the wash cycle, reverses through zero speed with a constant load torque. The constant may, though, need to be set close to one when power is first applied to allow the rotor to self synchronise to a known state. If the load torque quickly changes to zero at zero speed, such as with a friction load, and the motor speed is expected to rapidly go through zero, K_3 should be set closer to 1 or even higher. The setting for K_3 thus depends on the nature of the load and the speed of transition through zero speed. Another consideration is that the output of the second order integrator will drift if the controller motor parameter estimates do not match the actual motor parameters. The expected parameter errors puts a lower limit on the value of K_3 . For most applications, a value of K_3 of 0.3 has been found to be a good compromise.

In any case, if the load torque versus frequency profile of the load is fixed and known, it should be added to the inertial load model of equation (7) to reduce dependence on the torque disturbance feedback compensation system. Note that if the load torque cannot be correctly compensated for,

the value of the d axis current will need to be increased to ensure the rotor stays synchronised.

Direct Axis Current Setting

The final parameter setting that needs to be addressed for the controller design is the d axis current setting. To guarantee synchronism at zero speed this should be set at least high enough so that the resulting additional holding torque is greater than the peak torque error between the load model prediction and the actual torque. If the d axis current setting is too low, there is a chance the motor will lose synchronism at zero speed although it will usually resynchronise and start once the command torque reaches a high enough level. For a given d axis current setting, the peak pull-out torque is given by:

$$T_{\text{pull-out}} = \lambda_r i_d^* \quad (35)$$

The value chosen for current setting i_d^* at zero speed will probably be higher than this to provide a margin for error and possibly also to limit the initial torque angle error to provide a faster dynamic response at start-up. As speed is increased and the restoring torque produced by the back-EMF grows, the value of i_d^* can be reduced to reduce IR heating losses by multiplying it by a speed dependent function $F_D(\omega)$. The value of i_d^* will be given by:

$$i_d^* = i_{d0}^* F_D(\omega) \quad (36)$$

where i_{d0}^* is the value of i_d^* at zero speed. A suitable formula for $F_D(\omega)$ is:

$$F_D(\omega) = \frac{\omega_n}{|\omega| + \omega_n} \quad (37)$$

This is the same as the $F_0(\omega)$ function of equation (34). It will halve the value of i_d^* at the speed equal to the natural resonant frequency. Other formulae could be used depending on the application. For example, a ramp function where the value of i_d^* is reduced to zero at the natural resonant frequency can be used to further reduce IR heating losses.

For washing machine direct drive motors and other cost sensitive applications it may be necessary to set i_d^* to a high positive value during times when the motor is regenerating. This will cause extra power to be dumped into the motor's winding resistance preventing a net power flow into the inverter's DC bus, saving the cost of installing a DC bus energy dump circuit. A negative feedback controller could be added as suggested in [15] to regulate i_d^* according to the DC bus over voltage.

PWM Dead-Time Correction

If at least first order compensation is used for the torque and d axis current as shown in Figs 24 and 27, the average d and q axes currents will be well controlled and not influenced by PWM inverter errors, the largest of which is due to the effect of the PWM dead-time normally inserted to prevent top and bottom transistors in each inverter leg from conducting simultaneously. The compensation, though, has a very slow response time and without PWM error correction some deterioration in dynamic performance and even some instability could occur. If negative resistance or negative inductance is added to the inverter output impedance to improve dynamic performance, minimising PWM inverter errors is even more important.

To obtain accurate dead-time correction, a good method is to modify the pulse widths from direct measurement of the inverter voltage output PWM transition times as described in [16]. This method, though, requires extra hardware and may not be suitable for a low cost drive. An alternative but less accurate method is to just add a positive or negative offset depending on the

measured current polarity to the PWM modulation input for each phase to correct the distortion produced by the inserted dead-times [17,18]. This method can be implemented in software and is the method used in the experiments described in this paper. A disadvantage is that when the output current drops below the amplitude of the PWM ripple current this method over compensates for the required dead time correction, causing instability. A simple modification to minimise this effect is to stop the d axis current dropping below a minimum level sufficient to provide a bias current to limit this instability to an acceptable level.

Parameter Setting and Adaptive Parameter Adjustment

The feed forward torque controller relies on accurate estimates of the motor parameters for good dynamic performance. The parameter values can be obtained from the motor manufacturer's specifications or from off-line measurements, the method used for the experiments described in this paper, but they can also be obtained from on-line measurements and even adjusted adaptively while the motor is running.

Initial values of motor inductance and resistance can be measured off line by applying test voltages to the motor windings and measuring the currents. For the motor inductance, it is best to average the readings over different rotor positions to account for any rotor saliencies. These tests can also be done on line by using the PWM inverter to generate the test voltages.

Initial value for the peak rotor flux linkage can be found by measuring the motor open circuit winding voltage and frequency while the motor is spinning.

Initial measurement of the rotor inertia can be difficult particularly as the load inertia must also be included. A novel off-line method that can be used for a three-phase motor is to apply a constant current between two phases, start a transient oscillation of the rotor and measure the frequency of this oscillation by measuring the back-EMF waveform on the unconnected phase. The electrical 2-pole equivalent inertia can then be calculated using the following equation derived from the equation of motion (18):

$$J = \frac{I \lambda_l}{\omega_{osc}^2} \quad (38)$$

where ω_{osc} is the frequency of oscillation in radians per second, I is the line to line applied current and $\lambda_l = \sqrt{2} \lambda_r$ is the line to line peak flux linkage. The applied current must be large enough to produce enough restoring torque to minimise the effect of cogging torque and to overcome any mechanical damping. It is also important that the electrical angle deviation is small enough to ensure small signal conditions apply ($\Delta \theta \approx \sin \Delta \theta$).

Parameter adjustment while the motor is running is easy to implement with a feed forward torque control system. When the motor is stationary, the difference between the command d axis current and the measured d axis current can be used to calculate and correct the error in the estimated resistance. If the d axis compensator of Fig. 27 is used, the measured value of the motor resistance is given by:

$$R = \frac{i_d'}{i_d^*} \tilde{R} \quad (39)$$

Parameter adjustment for the motor inductance can be made by comparing the values of current i_d' for two different settings of the command current i_d^* at high speed. From equation (4), the q axis component of voltage at high speed ($\omega L \gg R$) and at steady state is given by:

$$v_q = \omega L i_d + \omega \lambda_r \quad (40)$$

If the d axis compensator of Fig. 27 is used, the d axis current error is held at zero and the following relationship, derived from equation (40), holds:

$$\tilde{L}i'_d + \tilde{\lambda}_r = Li_d^* + \lambda_r \quad (41)$$

Using two sets of readings at different current settings, the motor inductance can be calculated as follows:

$$L = \tilde{L} \frac{(i'_{d2} - i'_{d1})}{(i_{d2}^* - i_{d1}^*)} \quad (42)$$

where the 1 and 2 subscripts indicate the first and second measurement sets.

Parameter adjustment for the peak rotor flux linkage can be implemented using equation (41) assuming the estimated inductance is the same as the true inductance. The true flux linkage will then be given by:

$$\lambda_r = \tilde{\lambda}_r - \tilde{L}(i_d^* - i'_d) \quad (43)$$

The difference in the torque error between two different rates of acceleration can be used to calculate and correct the error in the estimated inertia, assuming the load torque remains unchanged. If the torque disturbance compensator of Fig. 28 is used, and the filtered version of the torque error measurement ΔT_m is used to smooth out torque ripples, then the true inertia would be given by:

$$J = \tilde{J} \left(\frac{(T_2^* - T_1^*)}{(T_2^* - T_1^*) - (\Delta T_{m2} - \Delta T_{m1})} \right) \quad (44)$$

where the 1 and 2 subscripts indicate the first and second measurement sets.

Motor Impedance Compensation

Motors with very low efficiency driving a high inertia load often have a winding resistance which is too high to obtain adequate damping at low speed. Also, motors having thin magnets and small air gaps to reduce cost may have inductances which are also too large to obtain adequate low speed damping. Some motors, such as direct drive washer motors, may have high resistance, high inductance and very high inertia loads. It can be very difficult to provide adequate damping for such motors.

One way to provide adequate damping is to electronically create negative resistance and/or negative inductance on the inverter output. Negative resistance is easily added by just making the added inverter resistance R_f in the feed forward block shown in Fig. 23 negative. Care must be taken to ensure the total motor plus inverter resistance never becomes negative else instability will result. Negative inductance can be added by modifying the feed forward block to that of Fig. 30 where L_N is the value of negative inductance added. Whereas the addition of the negative resistance is always stable provided the total resistance is positive, due to the low pass filter introduced by the motor's L/R time constant, the negative inductance loop must be stabilised by the addition of a single pole low pass filter. A possible placement of such filter with frequency roll off of ω_1 radians/sec is shown in Fig. 30. It could also be placed earlier in the i_d current measurement path since the roll off frequency is in most cases too high to affect the normal operation of the feed forward torque controller.

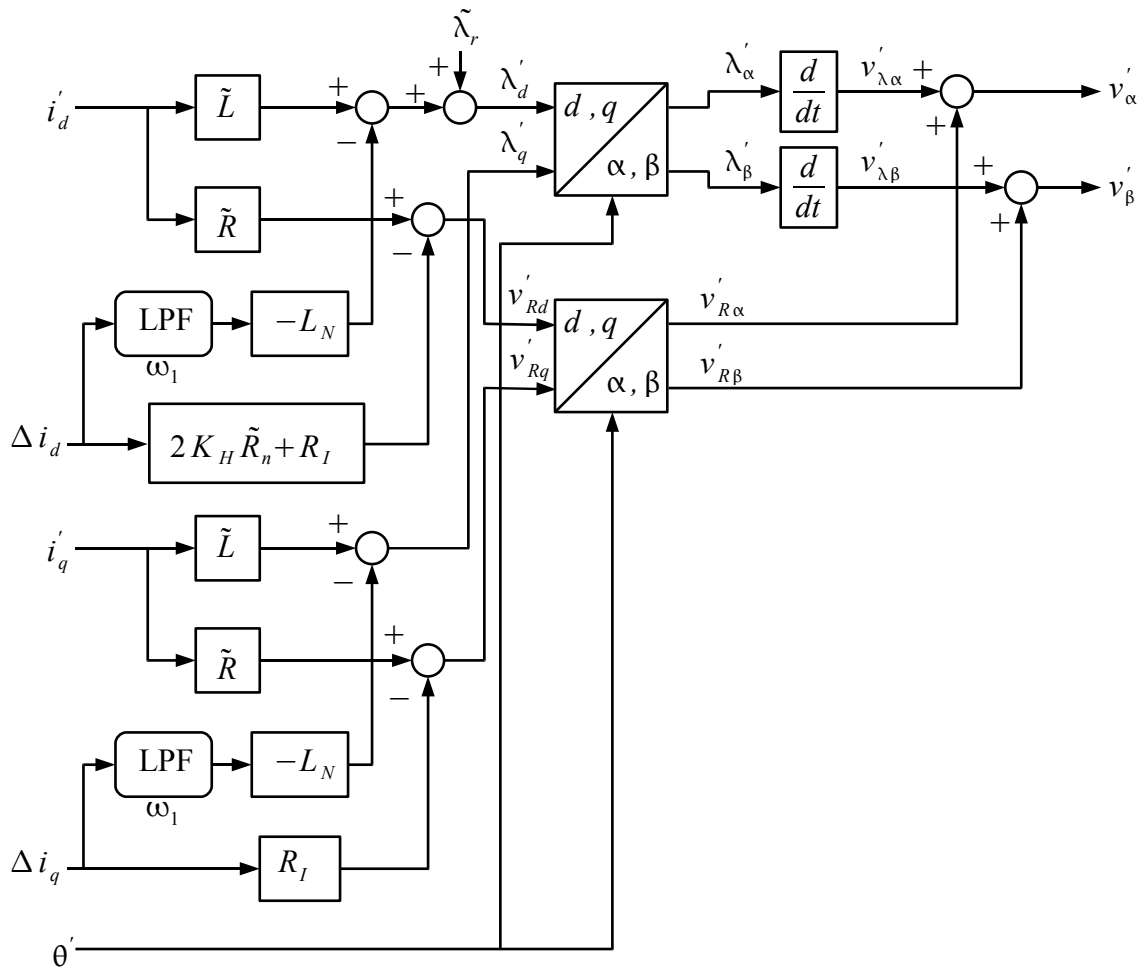


Fig. 30: Feed forward block with negative inductance added.

The simplified circuit of the negative inductance loop with Laplace transformed values, suitable for calculating parameters, is shown in Fig. 31. Resistance R_T is the total resistance of the motor and inverter, including any added negative resistance.

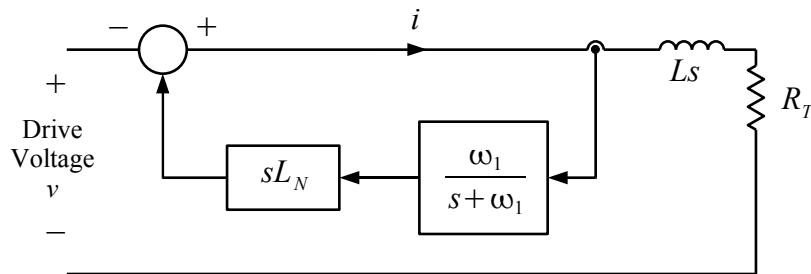


Fig. 31: Circuit of the negative inductance control loop.

By using Kirchoff's voltage law, the following loop equation is obtained:

$$v(s) = i(s) \left(R_T + Ls - \frac{L_N s \omega_1}{s + \omega_1} \right) \tag{45}$$

Rearranging and defining constant K_0 as:

$$K_0^2 = (R_T/L)/\omega_1 \quad (46)$$

the voltage to current transfer function is obtained:

$$\frac{i(s)}{v(s)} = \frac{1}{L} \left(\frac{s + \omega_1}{s^2 + s\omega_1 \left(\frac{L - L_N}{L} + K_0^2 \right) + K_0^2 \omega_1^2} \right) \quad (47)$$

The characteristic equation for this system is:

$$s^2 + s\omega_1 \left(\frac{L - L_N}{L} + K_0^2 \right) + K_0^2 \omega_1^2 = 0 \quad (48)$$

By comparing this with the universal characteristic equation for a second order system with damping factor ζ and natural resonant frequency ω_0 :

$$s^2 + s2\zeta\omega_0 + \omega_0^2 = 0 \quad (49)$$

the following formulae for damping and resonant frequency are obtained:

$$\omega_0 = K_0 \omega_1 \quad (50)$$

$$\zeta = \frac{1}{2K_1} \left(\frac{L - L_N}{L} + K_0^2 \right) \quad (51)$$

Rearranging equation (51) and completing the squares:

$$\frac{L - L_N}{L} = \zeta^2 - (K_0 - \zeta)^2 \quad (52)$$

Taking the negative square root solution (since $K_0 < \zeta$):

$$K_0 = \zeta - \sqrt{\zeta^2 - 1 + \frac{L_N}{L}} \quad (53)$$

The controller should be designed for a damping factor of at least 1. From equations (46) and (53), this limits the filter cut-off frequency to:

$$\omega_1 \geq \frac{R_T}{L \left(1 - \sqrt{\frac{L_N}{L}} \right)^2} \quad (54)$$

Alternatively, for a given filter cut-off frequency, the maximum negative inductance is limited to:

$$L_N \leq L \left(1 - \sqrt{\frac{R_T}{L\omega_1}} \right) \quad (55)$$

The maximum value of frequency ω_1 and thus the maximum negative inductance that can be inserted is limited by the maximum DSP sampling rate. Ideally, the cut-off frequency in Hertz should be kept to less than one tenth the sample rate to avoid interference from sampling effects.

Sampling Delay Compensation

The differentiation of output flux to get output voltage in the controller introduces a one sample delay. Also, the PWM unit between the controller and the motor usually introduces another one sample delay. These delays must be compensated for in order to obtain accurate current error

signals. A complete block diagram of the motor and controller with a speed control loop, showing the inserted compensating delays, is shown in Fig. 32. Compensating delays are inserted in the applied current signals and in the phase of the rotating reference frame. Without compensation the current error signals would be in error for motor frequencies approaching the sampling frequency, possibly causing instability.

Speed Loop Implementation

With an estimate of the rotor speed readily available from the feed forward torque controller, a standard proportional integral speed feedback loop is easily implemented. A suitable feedback loop is shown in block diagram form in Fig. 33. As shown, a torque limit of $\pm T_M$ is added to the output. The same limit is also applied to the integrator to prevent integrator wind-up. This works by ignoring any integrator input which would cause the integrator output to exceed the limit. This is the simplest method of preventing integrator wind-up. Other higher performance but more complex methods are available[19]. On a DSP platform, the PI controller would be implemented as a sampled digital filter. In such an implementation, it would be best to implement the proportional and integral parts separately to allow separate limiting of the integrator output.

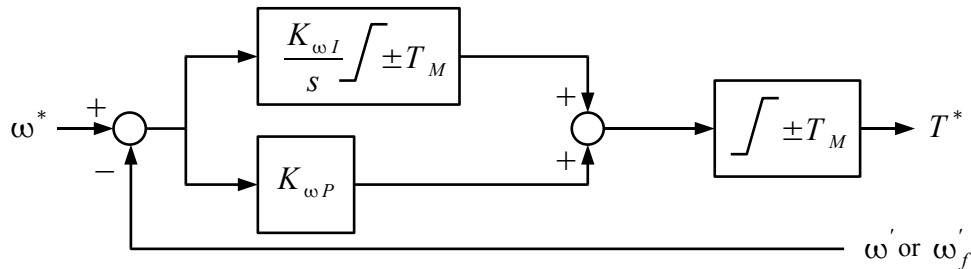


Fig. 33: Speed loop implementation.

The proportional and integral gains, $K_{\omega P}$ and $K_{\omega I}$ can be expressed using normalised parameters as follows:

$$K_{\omega I} = K_{\omega f}^2 \tilde{J} \omega_n^2 \tag{56}$$

$$K_{\omega P} = 2 K_{\omega d} K_{\omega f} \tilde{J} \omega_n \tag{57}$$

where $K_{\omega f}$ is the natural frequency of the second order system created by the PI speed loop as a proportion of the motor natural frequency ω_n and $K_{\omega d}$ is its damping factor. Using the damping factor and the normalised natural frequency instead of the proportional and integral gains to specify the speed PI controller has the advantage of directly specifying the speed loop's response characteristic. Normalising these parameters to the motor's natural frequency results in the speed loop's stability margins being independent of the motor and load characteristics.

For the speed feedback, either the direct feed forward applied frequency ω' or the filtered version ω'_f as shown in Fig. 29 can be used. The filtered version gives better stability margins but can cause a speed offset at low speed if there is an uncompensated torque error. It allows the speed feedback bandwidth to be set very high for very good torque disturbance rejection at high speed. If the direct version ω' is used, The feedback gain, particularly the proportional gain, can affect stability limiting feedback bandwidth. Also, if frequency ω' is used, an algebraic loop is introduced (no integral or delay terms in the path) via the speed feedback loop proportional path and the motor stabilisation path which will cause an error in a simulation. The algebraic loop can be prevented without affecting performance by inserting a low pass filter in series with the stability control term in Fig. 29. This filter is also recommended to prevent stability concerns caused by sampling. The cut-off frequency should be set high enough to not affect motor damping. Any value more than five times frequency ω_n but less than one tenth the sampling frequency would be reasonable. The load model plus stability control block of Fig. 29 with this filter added with a roll off frequency of ω_H is shown in Fig. 34. It is probably wise to put this filter in place for any practical implementation of the feed forward torque controller with speed feedback.

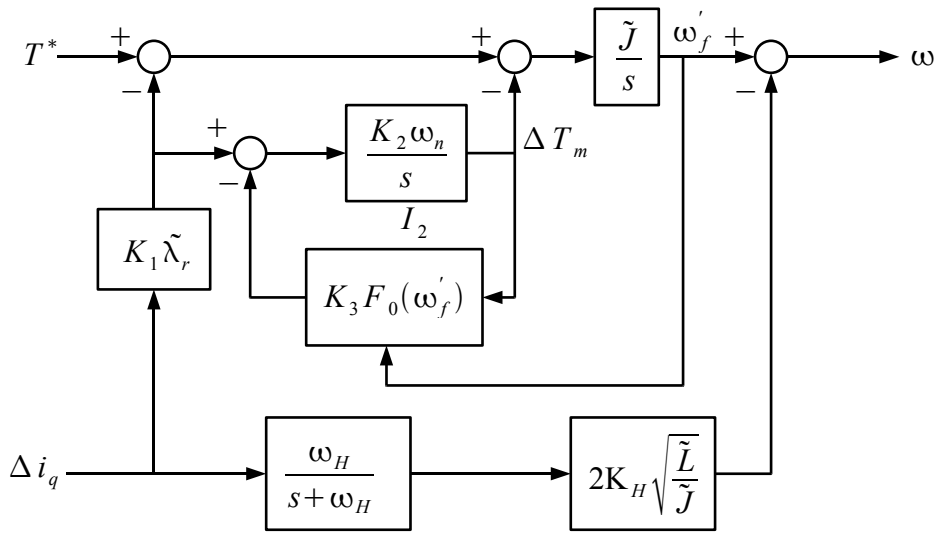


Fig. 34: Load model plus stability control block with a filter in the stabilisation path for improved speed feedback stability.

To analyse stability of the control system when the speed feedback uses the direct applied frequency ω' , refer to the complete diagram of the control system with the speed control loop shown in Fig. 32. There are two loops to be considered for stability analysis of the speed control system, one with negative feedback and one with positive feedback. The negative feedback loop is the direct loop formed by the speed proportional controller $K_{\omega P}$, current signals i'_q and Δi_q , the high speed damping compensator and the speed feedback signal ω' . The path of the positive feedback loop continues from current signal i'_q , through the torque feed forward block and the motor to motor current i_q then to current signal Δi_q . The gain of the negative loop is given by:

$$G_{\text{neg}} = K_{\omega P} \cdot \frac{1}{\lambda_r} \cdot 2 K_H \sqrt{\frac{\tilde{L}}{\tilde{J}}} \quad (58)$$

$$= 4 K_H K_{\omega d} K_{\omega f}$$

which is also the gain of the positive loop if the motor parameter estimates are accurate.

Ignoring sampling delays, if the estimated inductance used for the feed forward block match the actual motor inductance, the two loops cancel and no stability problems occur no matter how high the gain is set for the speed PI compensator. If the motor inductance is not correct, then it is important that the variation in inductance does not result in the overall gain at high frequencies, $G_{\text{neg}}(L/\tilde{L} - 1)$, remains less than +1 and preferably less than zero.

Because the torque control is instantaneous and the speed feedback signal is derived from an internal load model, the speed feed-back gain can be set to very high levels, much higher than for other sensorless control systems and even higher than for sensed control systems. This allows very fast speed response and very high load torque disturbance rejection. An upper limit on the setting of constant $K_{\omega f}$ of about 2 would be reasonable. If speed signal ω' is used instead of ω'_f , speed feedback gain does affect stability, particularly for large parameter errors, limiting the value of $K_{\omega f}$. Maximum usable values are best found by simulation and experiment. Typical values of $K_{\omega f}$ would be between 0.1 and 2 with damping $K_{\omega d}$ set to 1. The higher values can only be achieved if the estimate of motor inductance is accurate.

A compromise arrangement to obtain fast speed response with large parameter variations could be

to connect the speed feedback signal to the signal ω'_f via a high pass filter and to the signal ω' via a complementary low pass filter.

Adding the speed loop to stabilise the speed using feed forward torque control also has the effect of stabilising the output current at low and zero speed against errors in the PWM inverter output voltage and variations in the motor resistance, Any error in the q axis motor current results in a change in the applied torque via the torque disturbance corrector in the load model and stability control block shown in Fig. 28. This change is passed through to the applied speed via the inertia model integrator then to the torque command input via the speed feedback loop, resulting in the q axis current error being corrected. The result is that for low and zero speed steady state operation, the motor current is immune to inverter PWM and motor resistance errors, although these errors still affect dynamic performance.

Position Loop Implementation

For position control, an extra position feedback loop can be added around the speed feedback loop. Usually, position control is added by adding a proportional position loop around the above speed control loop. Such a control structure together with the transfer functions of the torque controlled motor drive assuming an inertial load is shown in Fig. 35. A slightly different structure which is commercially popular is the PDF (Pseudo-Derivative Feedback) control structure [20], also known as the PIV control structure (Proportional position loop, Integral and proportional Velocity loop) [21], shown in Fig. 36.

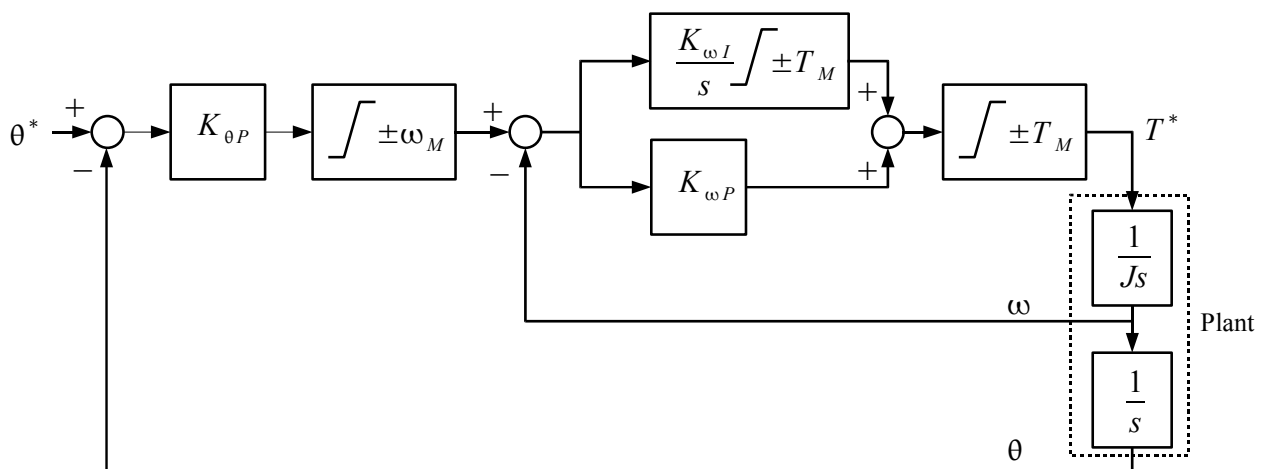


Fig. 35: Conventional position loop structure.

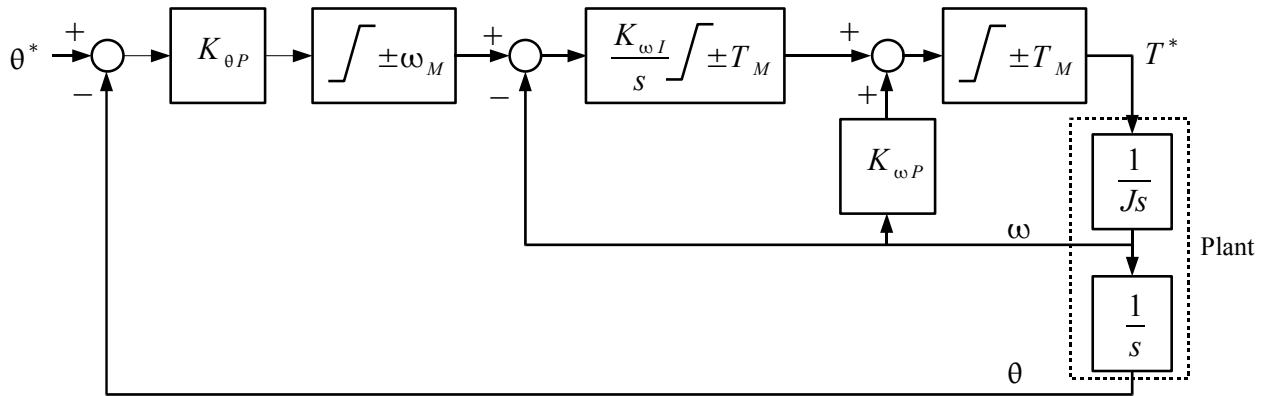


Fig. 36: PDF position loop structure.

These control structures are third order systems which causes several problems in use. First, under severe position step inputs where the torque limit is heavily saturated, the system goes unstable. Also, tuning is difficult with three control parameters to be chosen.

For a sensorless position control system using feed forward torque control, the much simpler and more robust dual proportional position control structure shown in Fig. 37 can be used. This is a second order system which is always stable under large step inputs. It is also much easier to tune with the two control parameters dictating the second order response curve. This structure is not normally used because a load torque offset at zero speed causes a steady state position error. This is not a problem when using feed forward torque control because any load torque offset is not detected at zero speed.

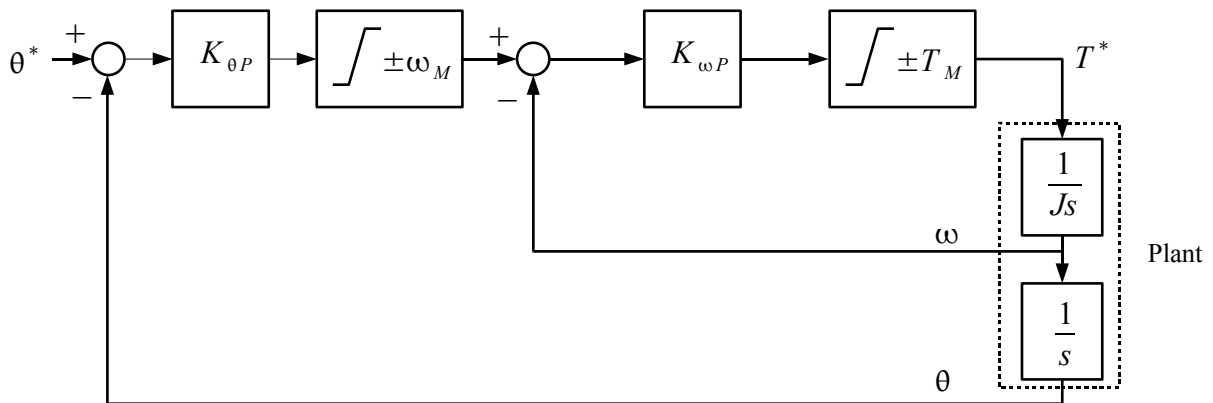


Fig. 37: Dual proportional position loop structure.

The transfer function for the dual proportional position controller as shown in Fig. 37 is given by:

$$\frac{\theta(s)}{\theta^*(s)} = \frac{\frac{K_{\theta P} K_{\omega P}}{J}}{s^2 + s \frac{K_{\omega P}}{J} + \frac{K_{\theta P} K_{\omega P}}{J}} \tag{59}$$

The characteristic equation for this system is:

$$s^2 + s \frac{K_{\omega P}}{J} + \frac{K_{\theta P} K_{\omega P}}{J} = 0 \quad (60)$$

Comparing this with the characteristic equation for a second order system (49), for a system natural frequency of ω_0 and a damping factor ζ , the two proportional gain settings are:

$$K_{\theta P} = \frac{\omega_0}{2\zeta} \quad (61)$$

$$K_{\omega P} = 2\zeta \omega_0 J \quad (62)$$

Suitable per unit parameter constants for natural frequency and damping are $K_{pf} = \omega_0/\omega_n$ and $K_{pd} = \zeta$.

An interesting application for FFTC with a position loop is as a replacement for the standard current feedback controller used in hybrid stepping motors. This would greatly improve their performance with no additional cost.

IV. Simulation and Tuning

Simulations of feed forward torque control are presented for two different motors: a 1 kW servo motor and a 500W direct drive washing machine motor. Experimental validation is carried out only for the servo motor. The simulation for the direct drive washing machine motor is included because with its very high stator resistance combined with a very high and variable load inertia it is likely to be the most difficult motor to control without sensors.

The simulations are carried out using Matlab and Simulink. To match a real motor controller as closely as possible, the controller is simulated with a fixed sample rate equal to the expected PWM sample rate while the motor itself is simulated at a high speed variable sample rate.

Servo Drive Simulation

The servo drive simulation incorporates a motor simulation of a 6 pole PMSM made by Lanzhou Electric Co, China. For the simulation, the 2-pole 2-phase equivalent parameters for the machine are used. The transformation from three phase to two phase currents and voltages used a scaling factor of $\sqrt{3/2}$ to preserve power. The parameters of the simulated motor are shown in Table 1. The inertia includes the equivalent inertia of the dynamometer load in the actual experimental setup. For this motor and load, the natural frequency is 91.4 rad/s and the natural impedance is 0.914 Ω .

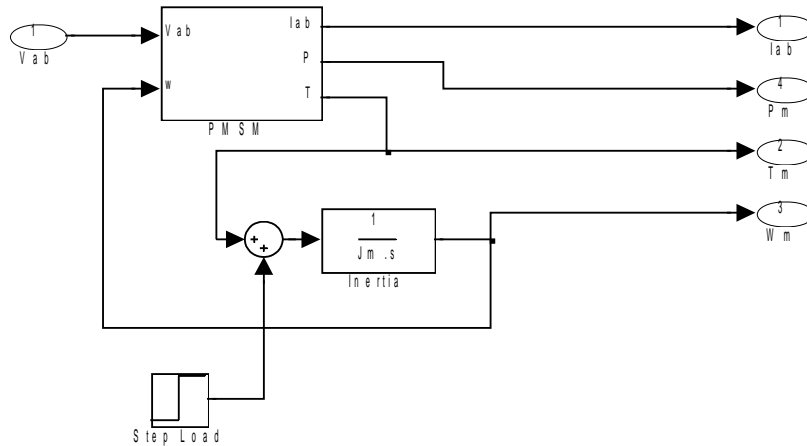


Fig. 39: Simulink model of PMSM and load.

The Simulink model of the controller block is shown in Fig. 40. All parameters for the controller is stored in the parameter block for convenience and for compatibility with the Dspace hardware implementation described later which uses the same Simulink model to generate its software code.

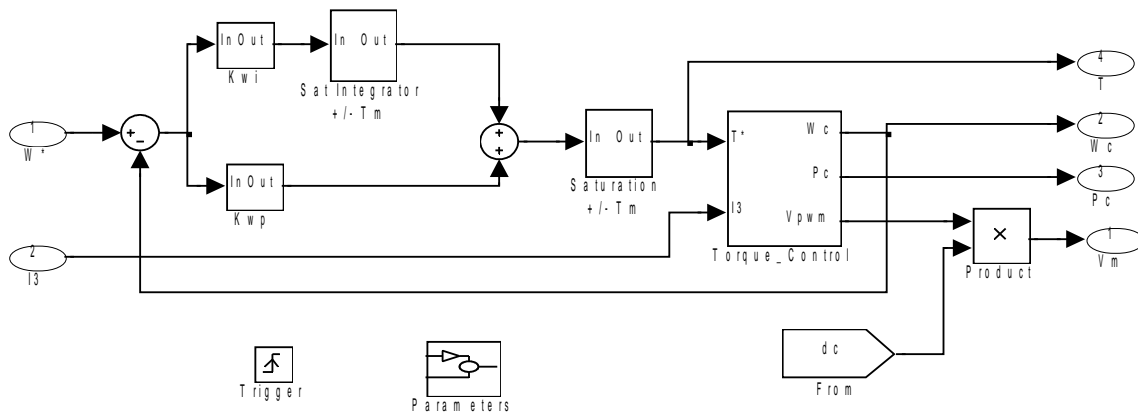


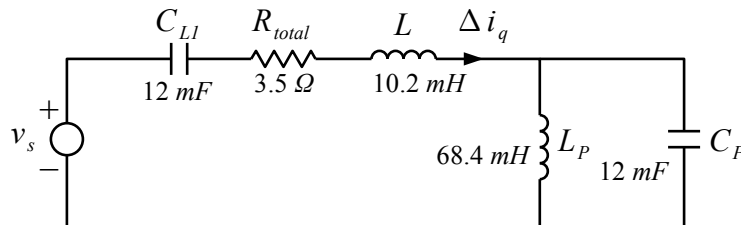
Fig. 40: Simulink model of the speed controller.

The controller parameters for the simulation were initially set to the values shown in Table 2.

Table 2. Controller Parameters for Servo Speed Control Simulation.

Parameter	Value	Description
f_s	5000 Hz	Digital Sampling frequency
T_M	1.5 Nm	Load torque limit
i_{d0}^*	2.5 A	d axis component of motor current at zero speed
K_H	2	High speed stability compensation gain constant
ω_H	500 Hz	Stability compensation filter roll-off frequency
K_1	1	Torque disturbance compensator 1 st order gain constant
K_2	0.5	Torque disturbance compensator 2 nd order gain constant
K_3	0.3	Torque disturbance compensator 2 nd order DC gain constant
$K_{\omega f}$	0.5	Speed feedback controller natural frequency normalised to ω_n
$K_{\omega d}$	1	Speed feedback controller damping factor
R_I	0	Added inverter generated output resistance
L_N	0	Added inverter generated negative inductance

The d axis zero speed command current is set to of 2.5 A, giving a pull-out torque of 0.43 N.m. At this current setting, the equivalent parallel inductance at zero speed shown in Fig. 26 is 68.4 mH, about seven times the motor series inductance. This allows fairly aggressive values for the parameters to be set to obtain fast response times. With the high speed damping gain K_H set to 2 the added series resistance is $2R_n$ or 1.8 Ω . Adding the motor resistance, the total series resistance is 3.5 Ω . The equivalent capacitance in Fig. 26 due to the inertia is 12 mF. Setting parameter K_1 to 1 adds an equivalent series capacitance of the same value. This setting of 1.0 for K_1 is on the high side providing a slightly oscillatory response but worked well in the simulation. Damping gain K_H is set high to 2 to restore damping lost due to high values of K_1 and K_H . The final zero speed approximate equivalent damping circuit is shown in Fig. 41. As for Fig. 26 the second order torque disturbance correction term is ignored.

*Fig. 41: Equivalent circuit for zero speed damping.*

The response of the current through inductance L_p , which is proportional to the rotor phase displacement, for a 1 Volt step input, obtained using the PSIM circuit simulation software, is shown in Fig. 42 for values of K_1 of 0.5 and 1. The response is slightly oscillatory for K_1 set to 1 and well damped for 0.5. In the servo drive simulation optimum performance was obtained with K_1

set to 1 and K_H set to 2 but in the experimental setup optimum performance was obtained with K_1 set to 0.5 and K_H set to 1, although performance variation between these values is only minor.

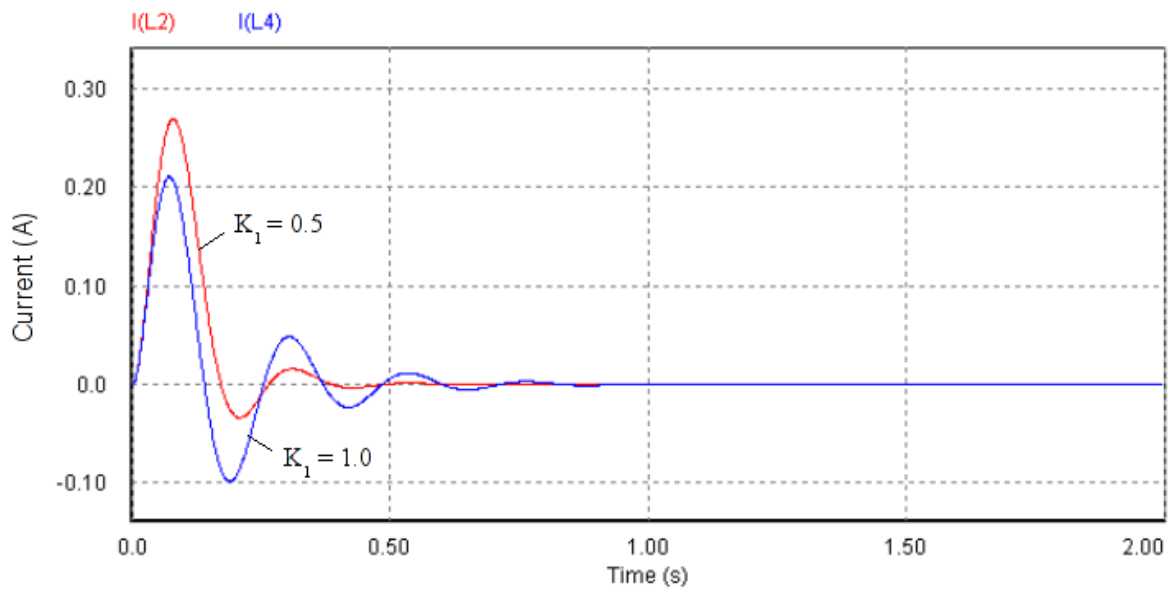


Fig. 42: Current through L_p for a 1 Volt step input.

The servo motor drive is first simulated with just an inertial load. The speed reference is stepped up to 500 rad/sec then back down to zero. The results of the simulation are shown in Figs. 43 to 46. There is some speed overshoot when the controller comes out of torque saturation which can be corrected by either profiling the speed command or using a more sophisticated anti-wind-up control. The torque response is virtually instantaneous and the phase error remains close to zero throughout the simulation. Note that as speed is increased the phase stepping in the controller due to sampling becomes more evident, causing a blurring of the waveform with the phase error returning to zero a each sampling point.

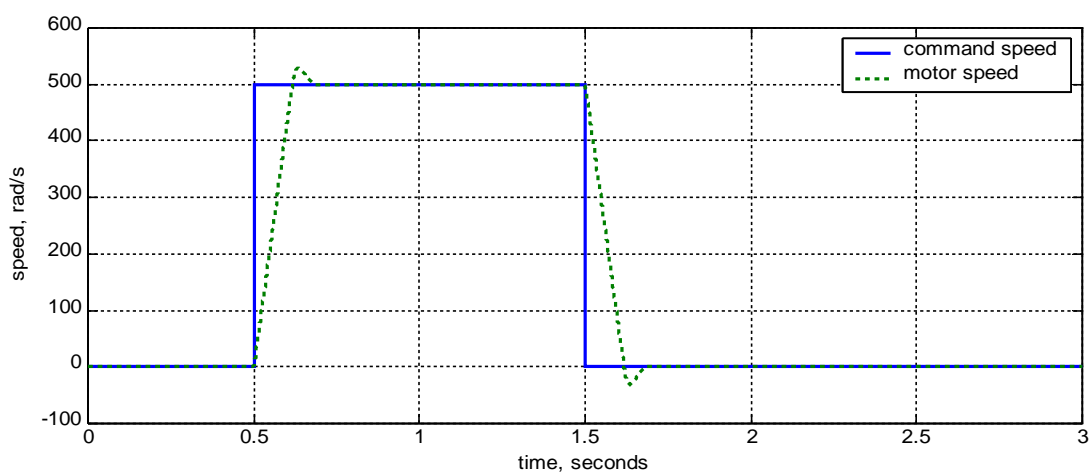


Fig. 43: Servo speed response from simulation.

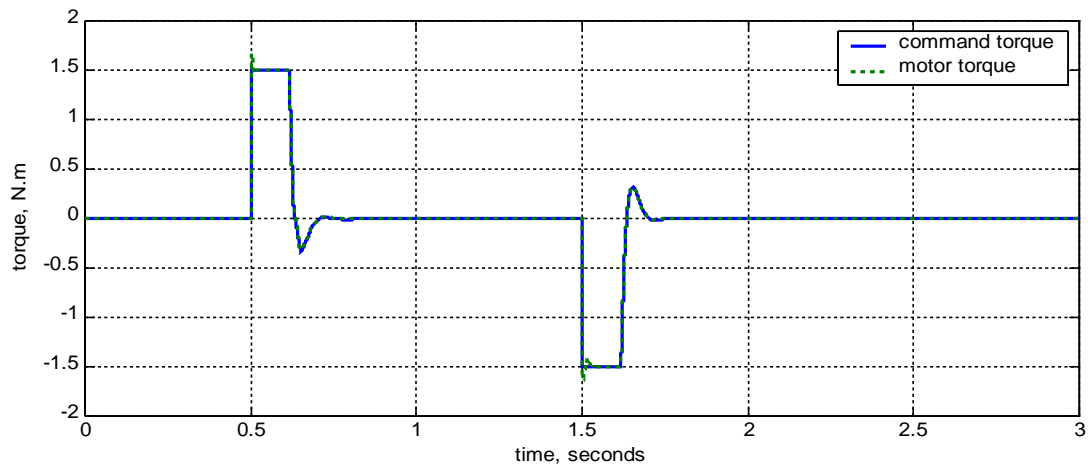


Fig. 44: Servo torque response from simulation.

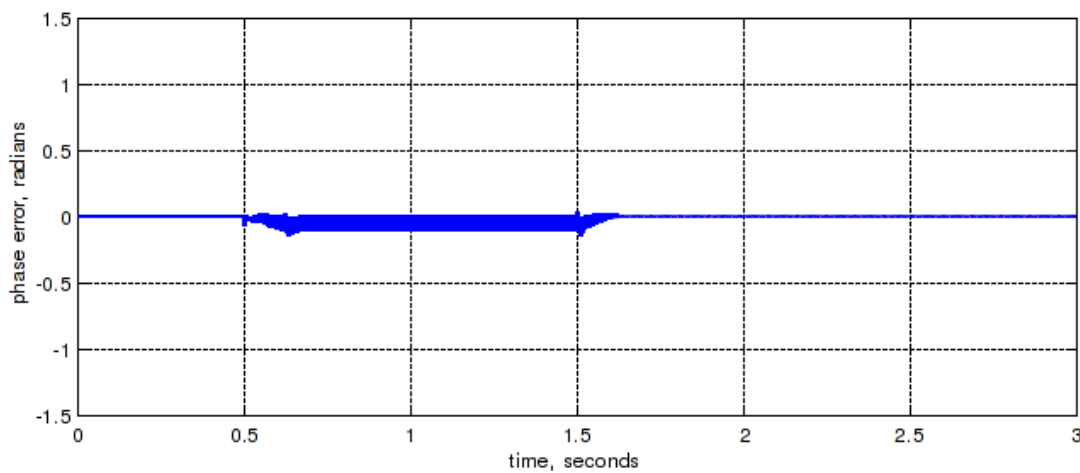


Fig. 45: Servo phase error from simulation.

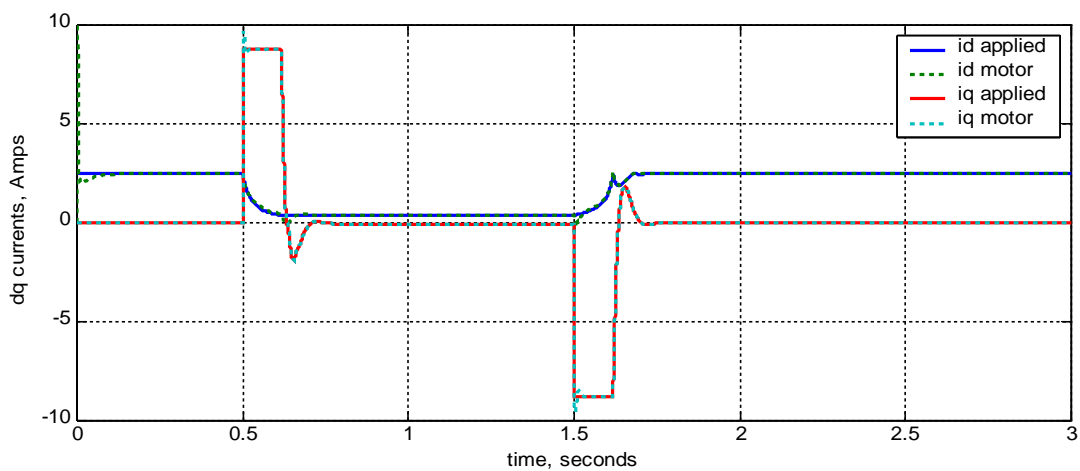


Fig. 46: Servo current waveforms from simulation.

The following simulation adds a disturbance torque of 0.3 N.m to test the response to a disturbance torque close to the pull-out torque. The 0.3 N.m disturbance torque is applied while the speed is at 500 rad/s and kept at that value to the end of the simulation. Also, to test the controller's ability to lock in the rotor phase the initial rotor phase error was set to 1.5 rad. The results of this simulation are shown in Figs. 47 to 50.

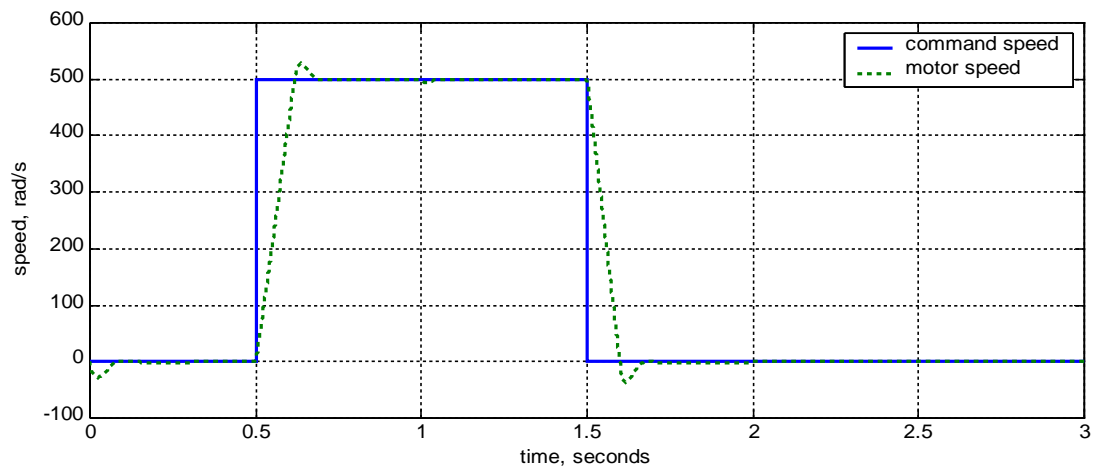


Fig. 47: Servo speed response with torque disturbance and initial rotor position error.

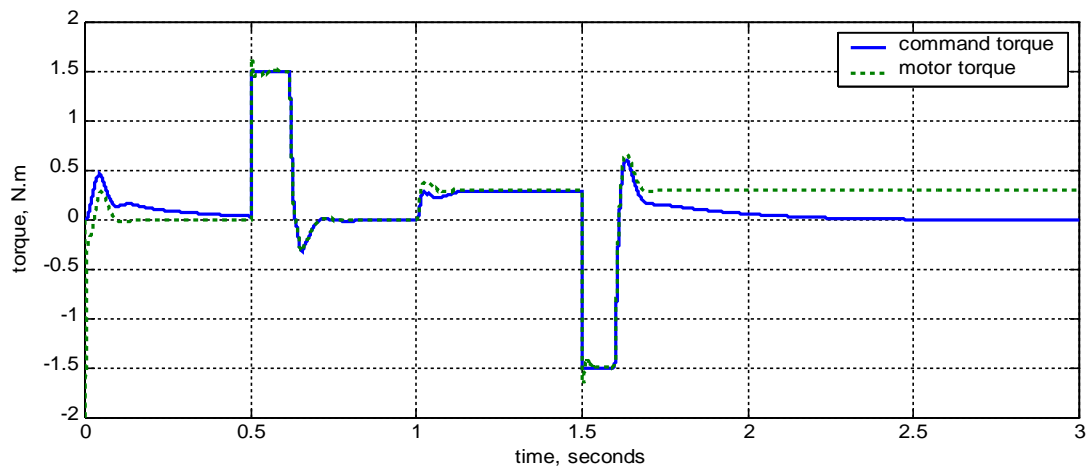


Fig. 48: Servo torque response with torque disturbance and initial rotor position error.

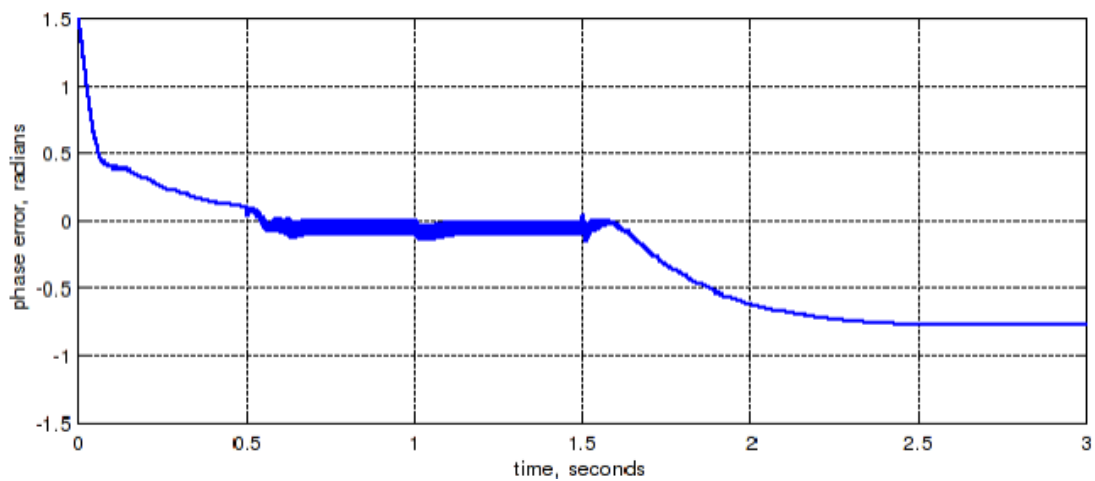


Fig. 49: Servo phase error with torque disturbance and initial rotor position error.

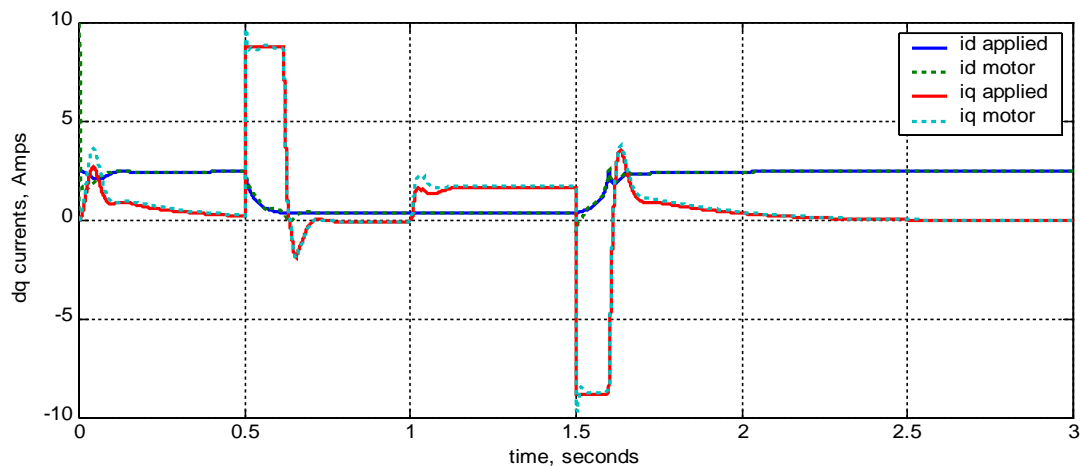


Fig. 50: Currents in the dq reference frame with torque disturbance and initial rotor position error.

The speed response shows excellent tracking ability at all speeds including very good torque disturbance rejection. The torque output graph shows near instantaneous response times and good torque tracking except as expected at low speed when torque output cannot be determined. At zero speed, the temporary torque memory effect where the controller remembers the last output torque at higher speeds can be seen. As explained previously, the rate of decay of this memory can be set by the second order torque parameter K_2 . The graph of phase error shows an initial rapid reduction in phase error until the second order torque disturbance effect takes hold to start a more progressive phase error reduction. Note that as soon speed is increased to the level where the back EMF could be used to determine actual rotor phase, the phase error rapidly drops to near zero. After zero speed is again reached at around 1.7 seconds, the phase error slowly settles to a large error consistent with a load offset torque close to the pull-out torque.

As shown in Fig. 50, except for the initial turn on transient, the d axis applied and actual currents match exactly for all speed and load conditions. The q axis currents also match closely except for brief transient conditions.

Parameter Sensitivity of Servo Drive

Generally a PMSM controller using feed forward torque control is very insensitive to motor parameter variations although if large parameter variations are expected the controller parameters should be chosen carefully.

For example, one of the most likely parameters to vary in a PMSM is the rotor flux level. Figs. 51 to 54 show the simulation results if the rotor flux is reduced by 20%. The results show that the d axis current which is normally very sensitive to changes in flux, is kept well controlled. Also, the speed response is nearly unchanged but when operating in torque limit during acceleration the motor torque is lower than the command torque by about 20% and is not as stable. As well, there is significant phase error when nearing zero speed in full torque limit. This is when the motor torque reduction must be taken up by the restoring torque provided from the positive d axis current.

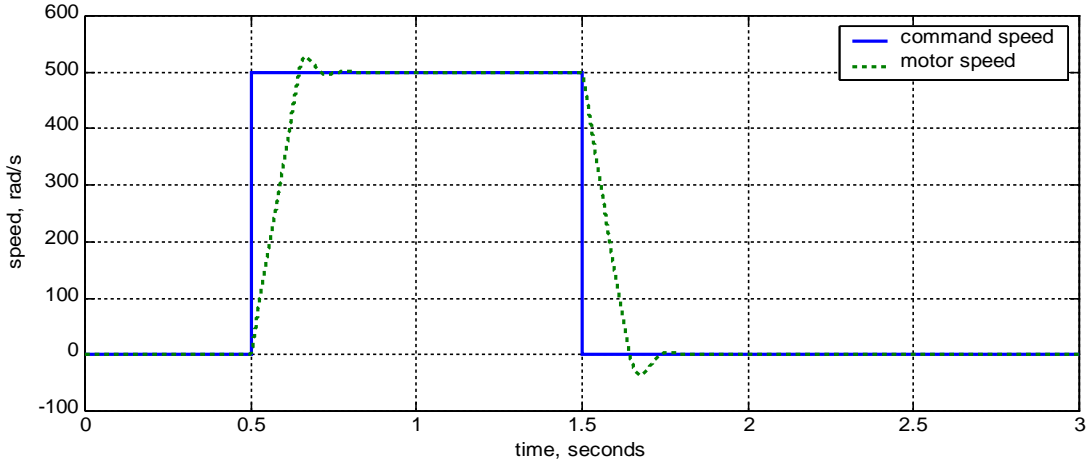


Fig. 51: Servo speed response with 20% rotor flux error.

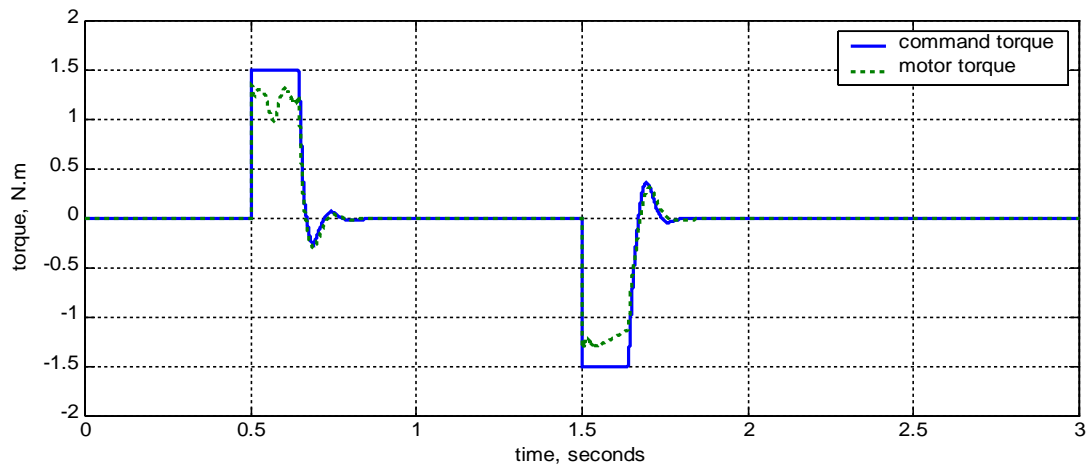


Fig. 52: Servo torque response with 20% rotor flux error.

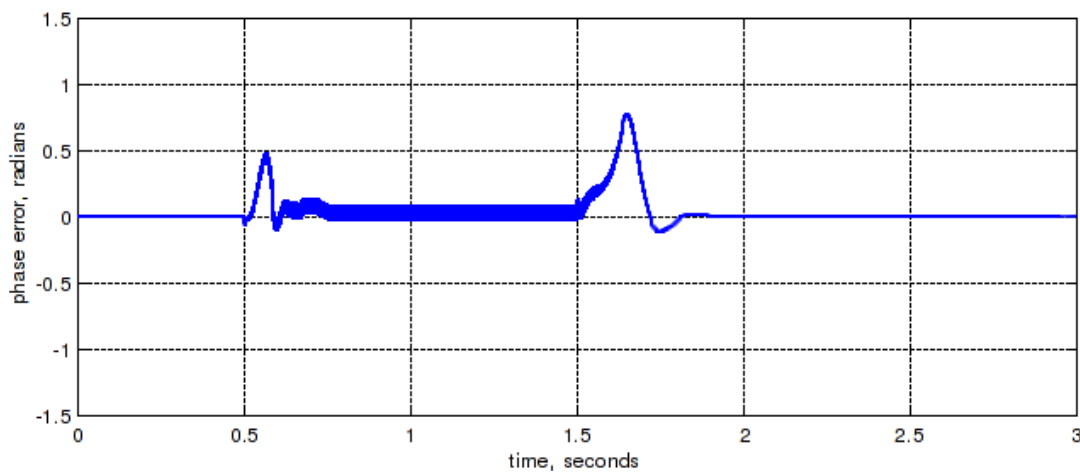


Fig. 53: Servo phase response with 20% rotor flux error.

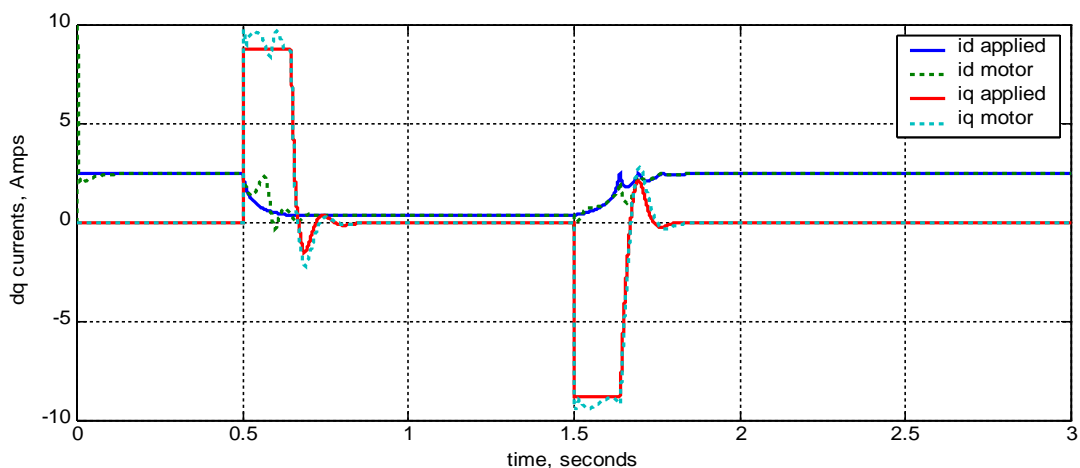


Fig. 54: Current waveforms in dq frame with 20% rotor flux error.

For the servo drive, the controller is even less sensitive to changes in stator resistance because this resistance is masked to some extent by the added series resistance produced by high speed damping. The greatest sensitivity is found from variations in the motor inductance. If the motor inductance is less than the controller estimate, the controller's estimate of changes in motor speed amplifies actual speed changes causing possible instability in the speed feedback loop. If inductance variations are

expected, the inductance estimate used in the controller should be set to the lower end of the expected range of inductance.

Washer Direct Drive Simulation

A direct drive motor for a top loading washing machine is a particularly difficult application for a sensorless speed controller [15, 22]. Winding resistance is very high to minimise cost and motor inductance is high due to the low flux of the typically ferrite magnets. Also, the load inertia is very high and varies greatly depending on the load. As well, the wash cycle speed profile is very demanding, requiring repeated rapid speed reversal at high torque. To add to the difficulty, the winding resistance can change by up to 30% and the rotor flux can change by up to 20% due to the motor temperature rise during the wash cycle.

Typical phase to neutral motor parameters of a three phase direct drive washer motor [15] are listed in Table 3. For the simulation of this motor, the equivalent two-phase, two-pole motor parameters are listed in Table 4.

Table 3. Parameters of the Direct Drive Washer Motor

Parameters	Value
Rated speed	150 rev/min
Rated power	500 W
Rated current	6 A
Number of poles	48
Back EMF constant λ_r	0.152 Vs
Phase resistance	4.6 Ω
d axis inductance	32 mH
q axis inductance	32 mH

Table 4. Parameters of the Simulated Washer Motor.

Item	Value
Phase	2 phase quadrature
Pole	2 pole
Rated frequency	377 rad/s (60Hz)
Rated current	7.35 A
Rated torque	1.5 N.m
Peak flux linkage	0.186 V.s
d-axis inductance	32 mH
q-axis inductance	32 mH
Phase resistance	4.6 Ω

The torque load on the motor over the wash cycle varies depending on the speed differential between the circular water flow and the bowl speed, but a reasonable approximation can be made by modelling the load as a fixed inertia. For a maximum 7 kg load in the machine used with the

above motor, the two pole equivalent load inertia is about 5×10^{-3} kg.m². With this inertia, the natural frequency for the above machine (λ_r/\sqrt{LJ}) is 14.7 rad/s and the natural impedance ($\lambda_r\sqrt{(L/J)}$) is 0.47 Ω . The machine has been simulated using this load and a typical wash cycle speed profile. The controller parameter settings are listed in Table 5. These are the same as those chosen for the servo drive except the load torque limit has been increased and a negative resistance has been added on the output to compensate for the rather large motor resistance. It was found adding the negative resistance is worthwhile to slightly improve the low speed response, although operation without it is possible reducing the need to compensate the inverter output for dead time distortion.

Table 5. Controller Parameters for Washer Speed Control Simulation.

Parameter	Value	Description
f_s	5000 Hz	Digital Sampling Frequency
T_M	3.0 Nm	Load torque limit
i_{d0}^*	2.5 A	d axis component of motor current at zero speed
K_H	2	High speed stability compensation gain constant
ω_H	500 Hz	Stability compensation filter roll-off frequency
K_1	1	Torque disturbance compensator 1 st order gain constant
K_2	0.5	Torque disturbance compensator 2 nd order gain constant
K_3	0.3	Torque disturbance compensator 2 nd order DC gain constant
$K_{\omega f}$	0.5	Speed feedback controller natural frequency normalised to ω_n
$K_{\omega d}$	1	Speed feedback controller damping factor
R_I	-3.5 Ω	Added inverter generated output resistance
L_N	0	Added inverter generated negative inductance

The results of the simulation are shown in Figs 55 to 58. The controller response is almost ideal. In particular, the inner feed forward torque controller tracks torque, phase and currents almost exactly.

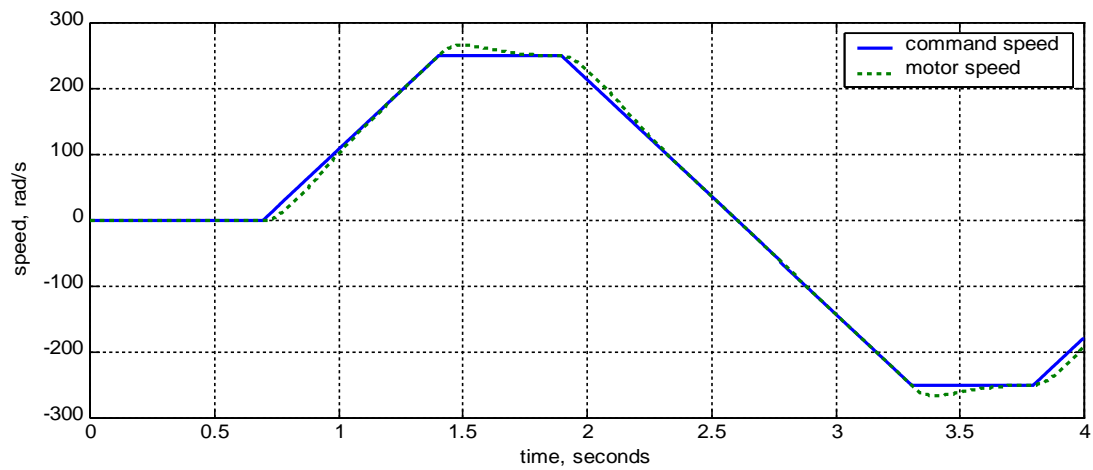


Fig. 55: Washer motor drive speed response from simulation.

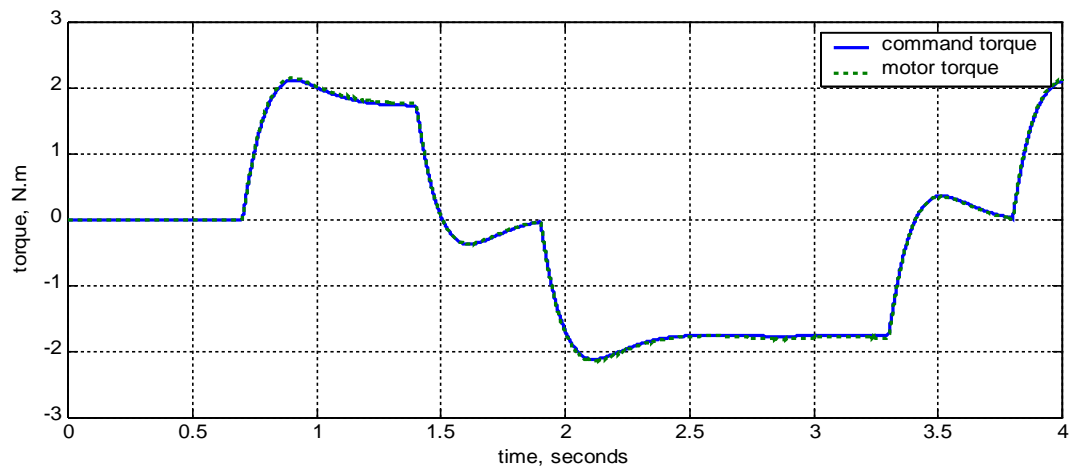


Fig. 56: Washer motor drive torque response from simulation.

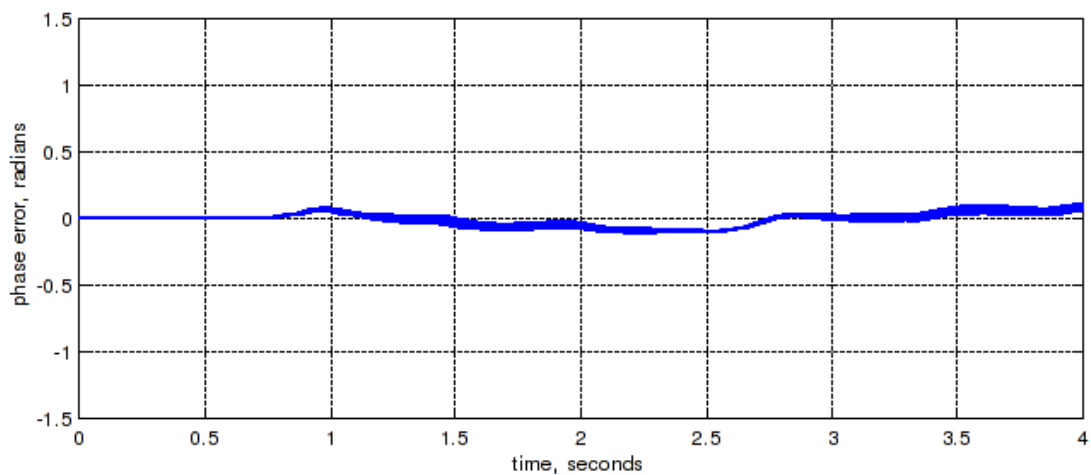


Fig. 57: Washer motor drive phase error from simulation.

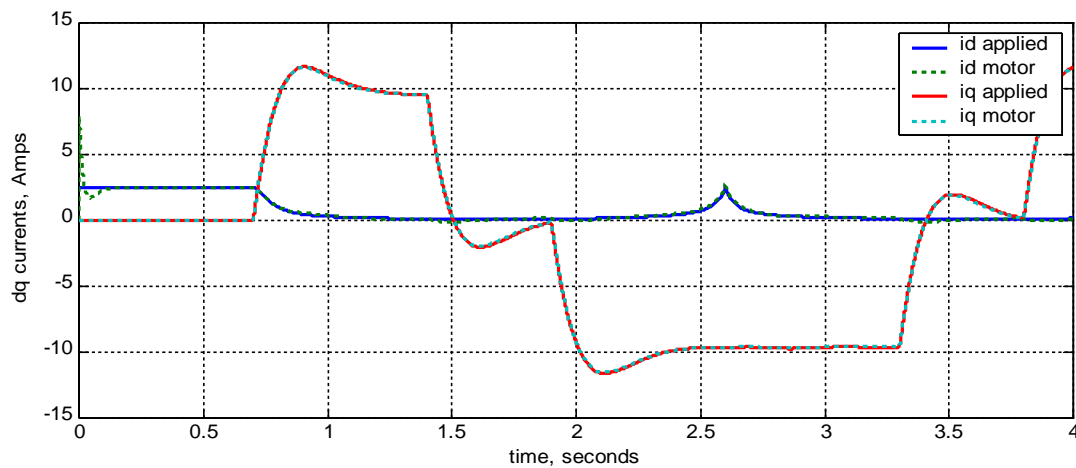


Fig. 58: Washer motor drive current waveforms from simulation.

Parameter Sensitivity of Washer Direct Drive

Other washer direct drive sensorless control schemes rely on estimating rotor position from the back EMF [15, 22]. These schemes must accurately estimate the voltage drop across the winding resistance in order to measure the back EMF, making them particularly sensitive to variations in resistance at low speeds. Accommodating these variations is very difficult when they can be up to 30% due to motor temperature variations.

For the simulated washer motor, the winding temperature may rise by 80 °C resulting in an increase in the winding resistance of 30% from 4.6 Ω to 6 Ω . During a full load wash cycle, the peak two phase equivalent current is 8A giving a resistance voltage drop of 48V when hot, yet the peak back EMF is only 47V at maximum wash speed, making measurement of the back EMF especially near zero speed extremely difficult.

For a controller using FFTC, the sensitivity to winding resistance is eased somewhat. The main problem now is the effect of the temperature induced variation in winding resistance on the low speed motor damping. For the simulated washer motor, the ideal damping resistance is around 1 Ω but the actual resistance varies from 4.6 Ω to 6 Ω . In simulation, it was found that this range can just be accommodated if the estimated resistance is set to 6 Ω and the inverter resistance R_I is set to -6 Ω , the most negative value which could be set whilst maintaining good stability. The estimated resistance is set to the high end of the range to ensure motor torque is over rather than under compensated. Speed response for the worst case situation when the motor is cold as shown in Fig 59. is only marginal. In a practical controller, a software thermal model of the motor, combined with initial motor resistance measurement at rest using the d axis current would easily allow tracking of the winding resistance to within 10%, greatly improving controller performance under temperature variation,

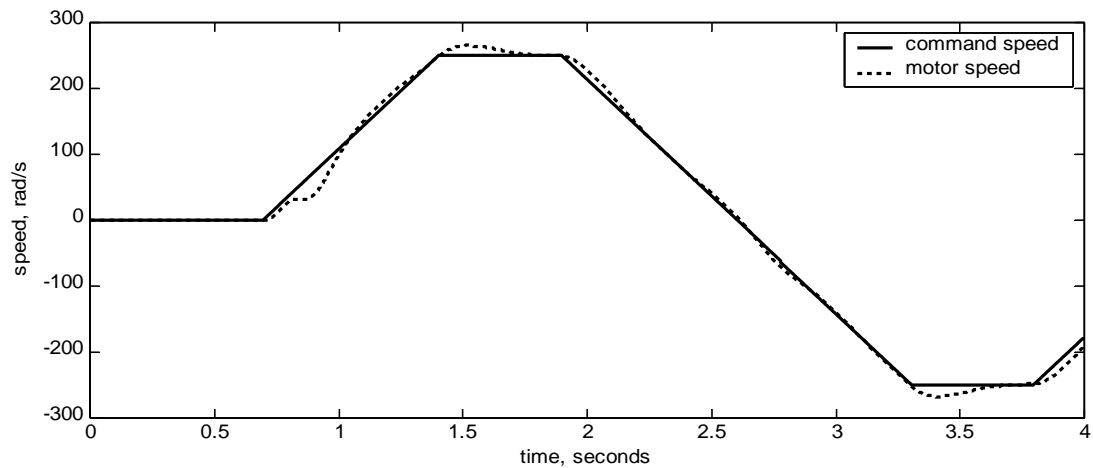


Fig. 59: Washer motor drive speed response with 30% change in motor resistance.

To test sensitivity to variations in washer load, the actual equivalent load inertia in the simulation was reduced to $4 \text{ kg}\cdot\text{m}^2$, the expected value for a washer load of 3 kg. Controller parameters were kept as shown in Table 5. The results of the simulation are shown in Figs. 60 to 63. The main effect of the reduced inertia can be seen in the phase plot of Fig. 62. On initial acceleration after standstill the motor phase advances due to more torque being applied than required. This error reduces as speed is increased allowing the controller to detect and correct the torque error.

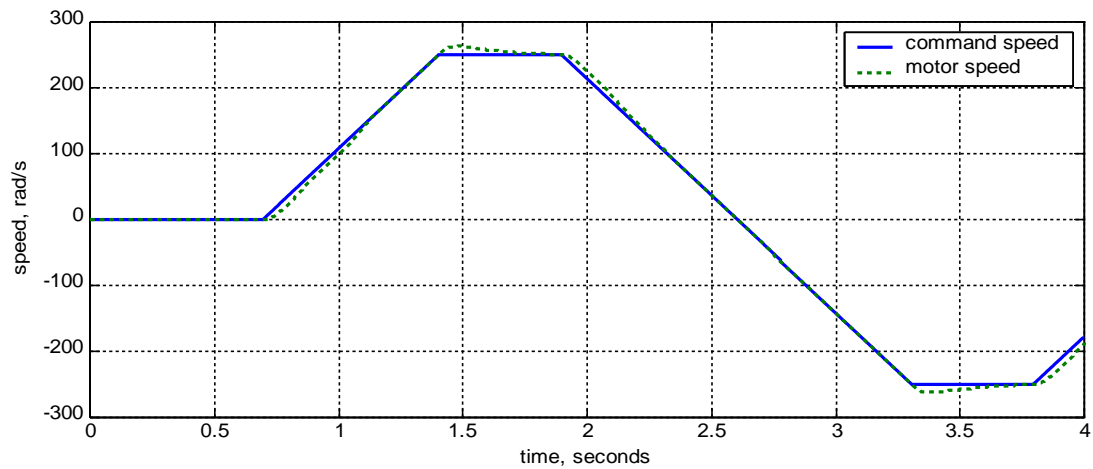


Fig. 60: Speed response with 20% load error.

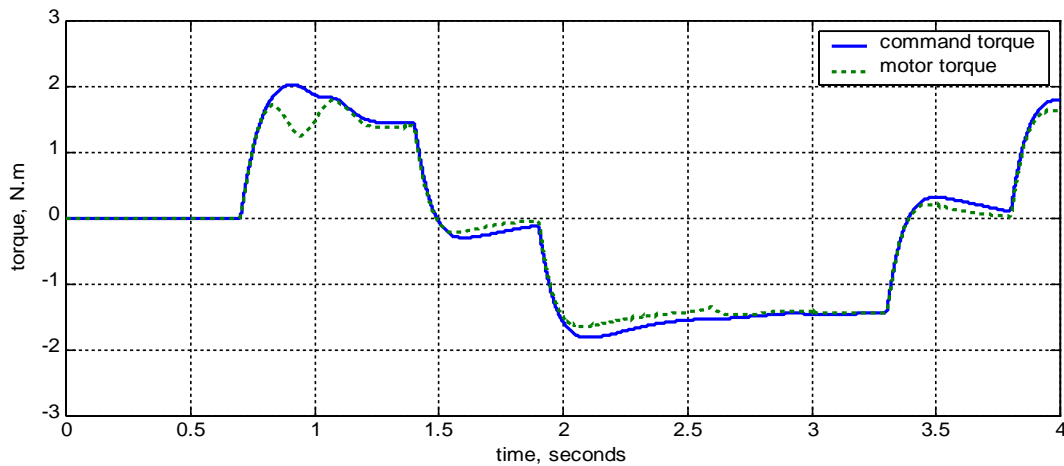


Fig. 61: Torque response with 20% load error.

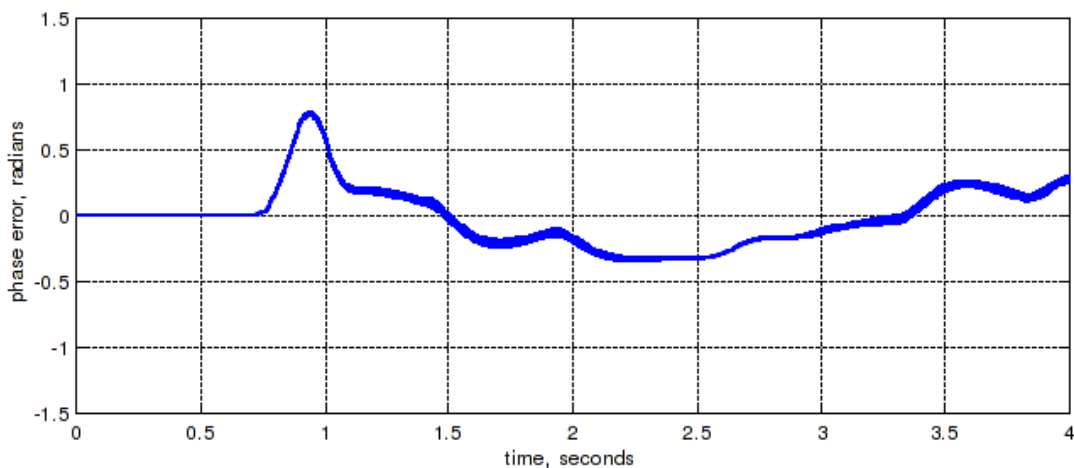


Fig. 62: Phase error plot with 20% load error.

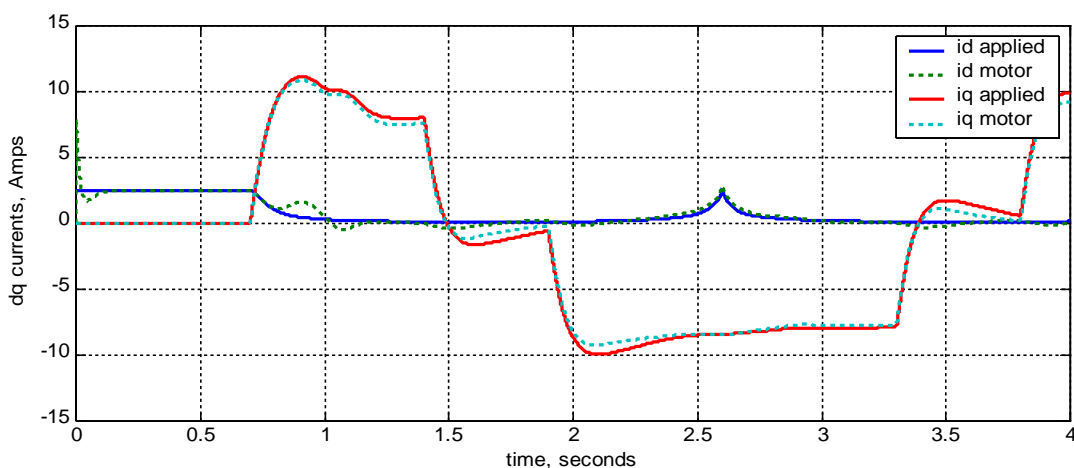


Fig. 63: Current waveforms with 20% load error.

Note that the torque error is much larger on the initial speed increase from zero compared with subsequent speed reversals through zero. This is because the second order component of the torque disturbance compensator "remembers" the load torque measured at high speeds as the speed reverses through zero. With this mechanism, even larger load torque errors can be accommodated if the initial rise in motor speed is slowed until the speed rises to a sufficient level to enable the load

model torque disturbance estimator to determine the true load torque. This feature, unique to feed forward torque control, is particularly useful for a cyclic reversing drive such as a washing machine direct drive.

Similar errors in other motor parameter estimates can also be accommodated. To reduce the chance of stalling the motor, it is much better that the error estimated result in an over torque and subsequent phase advance being applied to the motor rather than a phase retard.

With motor flux errors, the washer controller stability was found sensitive to a motor flux reduction but not to a motor flux increase of 20%. The motor flux estimate used in the controller should be set to the low end of the expected range, or alternatively, the flux estimate can be adjusted adaptively online, which is easy to do during the speed "plateau" period.

The estimate used for the motor inductance should be set to the low end of the expected range as was found for the servo drive simulation.

Difficult Loads

In this section, how FFTC handles some difficult loads which often occur in practice is examined through simulation. Two types of loads are investigated: step load torque at zero speed and Coulomb load torque. The previous servo motor simulation is used but with the following control parameter changes for improved handling of load torques at zero speed:

Table 6. Controller Parameters for Servo Speed Control Simulation.

Parameter	Value	Description
i_{d0}^*	7.6 A	d axis component of motor current at zero speed
K_H	1	High speed stability compensation gain constant
K_1	0.5	Torque disturbance compensator 1 st order gain constant
K_3	0.3	Torque disturbance compensator 2 nd order DC gain constant
R_l	-1	Added inverter generated output resistance

The d axis command current at zero speed was increased to 7.6 A to allow the drive to hold torques of up to 1.3 Nm at standstill. A negative resistance of 1.0 Ω was added to improve zero speed stability in the presence of a high d axis current. Other parameters were also adjusted slightly for better stability/performance compromise for difficult loads.

The results of a simulation run where a step torque of 1 Nm is applied with the speed set point kept at zero are shown in Figures 64-66. A load torque step of 1 Nm is applied at time 0.2 seconds. This results in the phase error between the controller applied rotor phase and the actual rotor phase to build up to about 0.8 radians. This phase error and the controller's d axis current causes a restoring torque to counter the 1 Nm load torque bringing the motor speed back to zero. The initial change in speed when the torque step is first applied results in the controller applying a damping current to the q axis to slow down and damp the rate of change of the rotor phase.

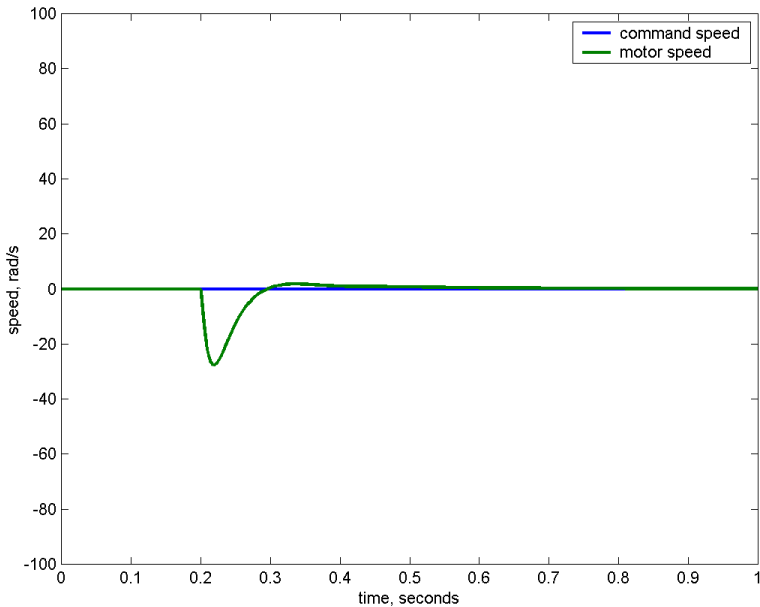


Figure 64: Speed response to a 1 Nm step load at standstill.

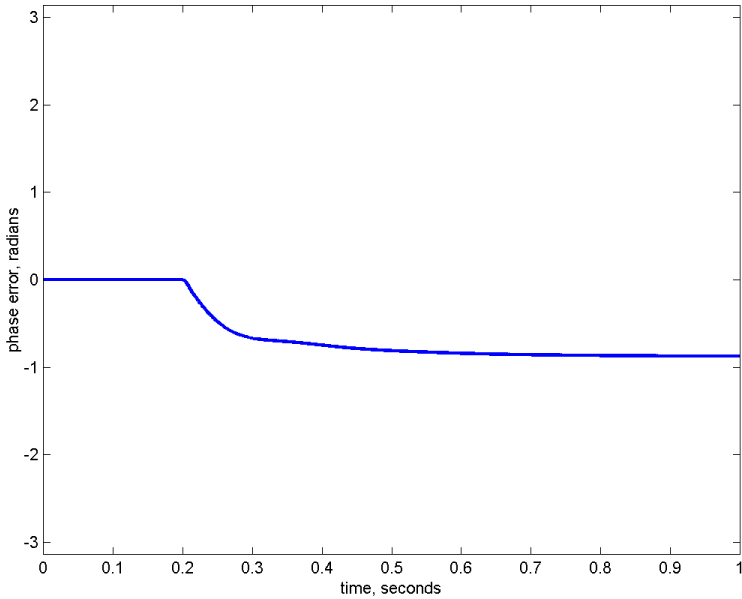


Figure 65: Phase error to a 1 Nm step load at standstill.

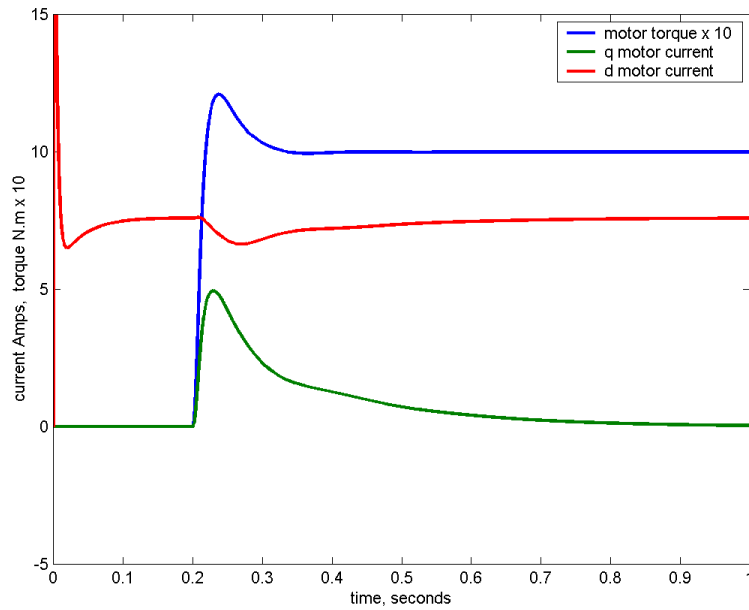


Figure 66: Torque and current for a 1 Nm step load at standstill.

The results of a simulation run where a Coulomb load of 1 Nm is applied are shown in Figures 67-68. This applies zero torque at zero speed but immediately steps to 1 Nm when the speed rises above zero. As speed is increased, the presence of back EMF allows the controller to measure the load torque and apply a compensating q axis current and torque. This initially rises to above the command torque from the speed controller to bring the phase error quickly to near zero. As speed rises further, the d axis set-point current is reduced towards zero as it is no longer needed. This ensures maximum efficiency at high speed.

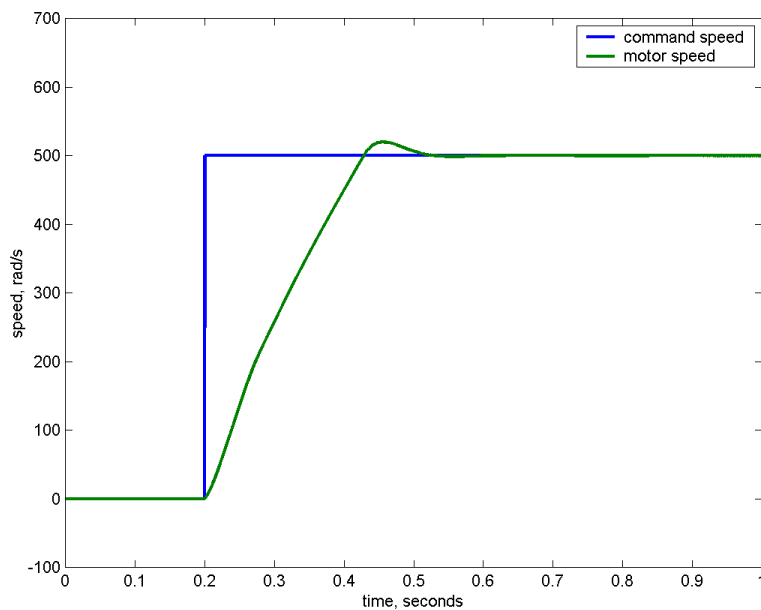


Figure 67: Speed response with a 1 Nm Coulomb load.

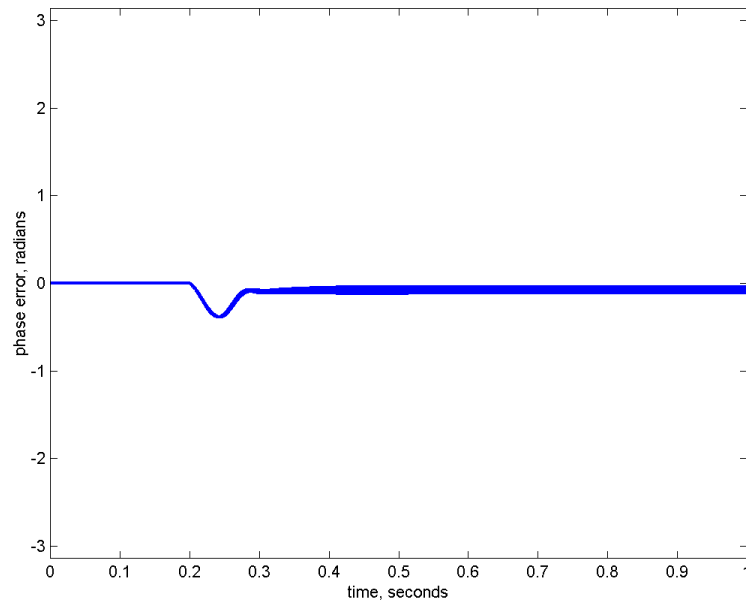


Figure 68: Phase error with a 1 Nm Coulomb load.

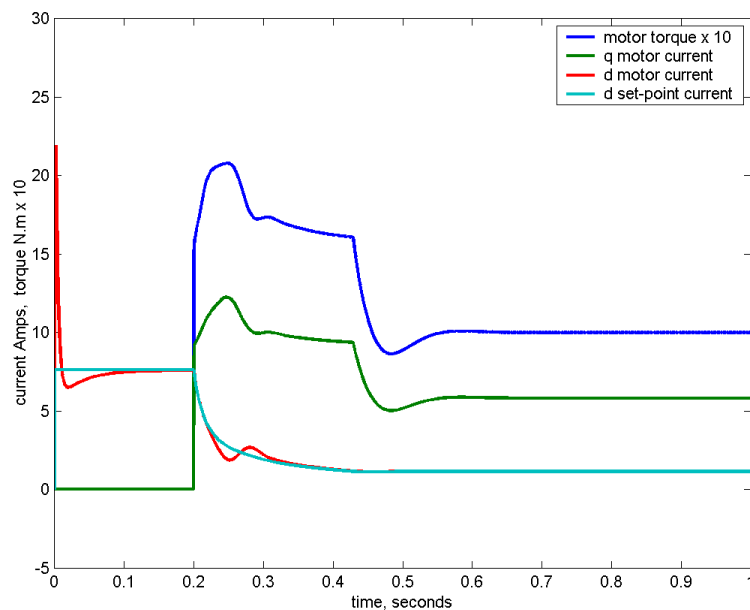


Figure 69: Torque and current for a 1 Nm Coulomb load.

V. Experimental Verification

System Description

A PM synchronous servo motor similar to the simulated motor was connected up to a Magtrol magnetic hysteresis dynamometer for testing the new controller. The FFTC algorithm was run on a dSpace DS1104 motor control board using a download of the same Simulink software used for the simulation. The algorithm was operated in the speed control mode with an outer speed PI loop with speed feedback from the controller frequency ω' . The DS1104 board was connected to the motor

via a Semikron Skiip based inverter module supplied from a regulated 200V DC source. The inverter operates at 5 kHz PWM carrier frequency which is synchronised with the 5 kHz controller sampling. The PWM cross-over dead time to prevent shoot-through is set to 1 microsecond. Ninety percent of this dead time is compensated for in the controller by the simple method of adding a positive or negative offset to each phase of the PWM modulation input depending on the measured current polarity of that phase. Compensation to 100% is not possible due to the risk of instability. This method of compensation can be unstable at low currents due to discontinuous output current. To prevent this, the d axis current was prevented from dropping to below 1 A.

The settings were used in the controller for the experiment are different to those used in the simulation. The actual test motor has an actual measured phase inductance of 13 mH rather than the 10 mH used in the simulation. For the controller, it was found slightly better performance with less feed forward torque error was obtained with the controller estimation of motor inductance set to 15 mH. Due to the mechanical resonance caused by the motor to dynamometer coupling, the speed feedback normalised natural frequency $K_{\omega f}$ had to be reduced to 0.2 and the damping factor $K_{\omega d}$ had to be increased to 1.5.

Equipment Used

Motor:

Manufacturer: Lanzhou Electric Co

Name Plate Ratings:

Torque: 4.5 N-m

Speed: 2000 rpm (209.4 rad/s)

Current: 6.5A

Voltage: 128 V line to line

Poles: 6

Per Phase Resistance: 1.7 Ohms

Per Phase Inductance: 13 mH

Total motor plus load inertia: 3×10^{-3} kgm²

Load:

Magtrol magnetic hysteresis dynamometer with a shaft mounted torque meter (not used) between the motor and dynamometer. Two flexible couplings, one on each end of the torque meter are used.

This dynamometer can supply a fixed torque load at all speeds down to zero, but not at zero.

Inverter:

Three phase PWM inverter built from a Semikron Skiip inverter module and a Semikron gate drive module. The DC input is supplied by a laboratory power supply.

Rating: 200VDC bus, 10A peak output.

PWM carrier frequency: 5 kHz

Dead time delay setting: 1 microsecond

Controller:

dSpace DS1104 controller board mounted in a Dell PC.

This board incorporates a Texas Instruments TMS320C240 motor controller DSP and a Freescale Power processor and runs with software code compiled directly from Simulink.

The software runs at a fixed sample rate of 5 kHz synchronised with the PWM carrier.

Controller Settings

The settings for the controller parameters differ slightly from those used in the simulation. a complete list of the parameters is shown in Table . As in the simulation, these are the two-phase, two-pole equivalent settings.

Table 7. Controller Parameters for Servo Speed Control Simulation.

Parameter	Value	Description
f_s	5000 Hz	Digital Sampling frequency
T_M	1.5 Nm	Load torque limit (equivalent to mechanical 4.5 Nm)
i_{d0}	2.5 A	d axis component of motor current at zero speed
K_H	1	High speed stability compensation gain constant
ω_H	500 Hz	Stability compensation filter roll-off frequency
K_1	0.5	Torque disturbance compensator 1 st order gain constant
K_2	0.5	Torque disturbance compensator 2 nd order gain constant
K_3	0.3	Torque disturbance compensator 2 nd order DC gain constant
$K_{\omega f}$	0.2	Speed feedback controller natural frequency normalised to ω_n
$K_{\omega d}$	1.5	Speed feedback controller damping factor
R_I	0	Added inverter generated output resistance
L_N	0	Added inverter generated negative inductance
$\tilde{\lambda}_r$	0.171 Vs	Estimated peak rotor flux linkage
\tilde{R}	1.7 Ω	Estimated per phase resistance
\tilde{L}	15 mH	Estimated per phase inductance

Performance Tests

The UTS sensorless control algorithm, which is a torque control algorithm, is incorporated into a speed control loop to allow speed input tests. The speed loop response time is set as short as

possible without exciting the shaft resonances that exist between the motor, couplings and load. The results of each test is shown in a graph showing the input reference speed, the actual motor speed, the torque reference input to the torque controller and the actual motor torque. The actual motor speed and torque are taken from the control algorithm with the torque calculated directly from the measured q axis motor current and a knowledge of the rotor flux using the formula:

$$Torque = i_q \times \tilde{\lambda}_r \times p \tag{63}$$

where p is the number of pole pairs, which is 3 for the test motor.

Step Speed Response at Zero Speed

Figures 70 to 73 show the response to a step speed input, both from zero to 1600 rpm and from 1600 rpm to zero at controller torque limit settings of 1.5 and 4.5 Newton-metres. These figures also show the step torque response. Note that the torque and speed responses are very well behaved and are independent of speed. Torque and speed response at zero speed is the same as at 1600 rpm. Note that the output torque response to a step in the torque reference is virtually instantaneous. Unlike other sensorless control methods, there are no control limitations near zero speed.

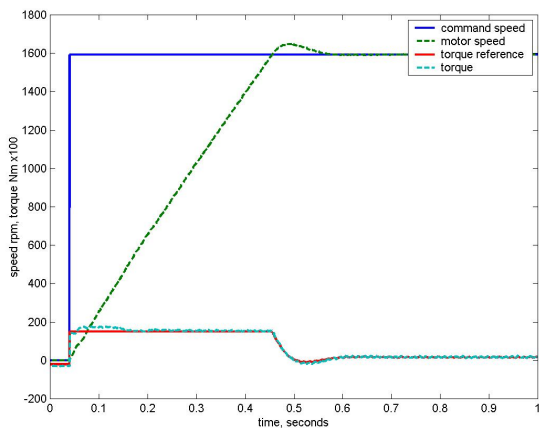


Figure 70: Step speed response. 0 to 1600 rpm, torque limit set to 1.5 Nm.

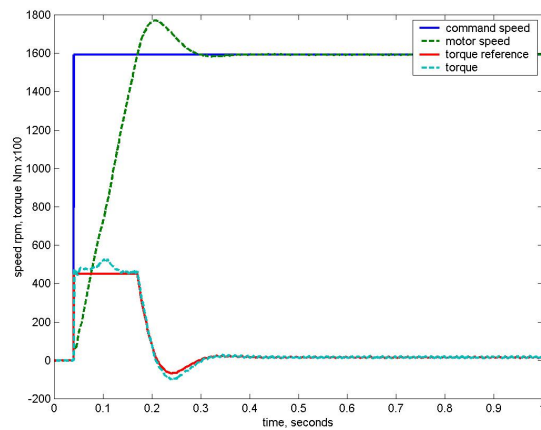


Figure 71: Step speed response. 0 to 1600 rpm, torque limit set to 4.5 Nm.

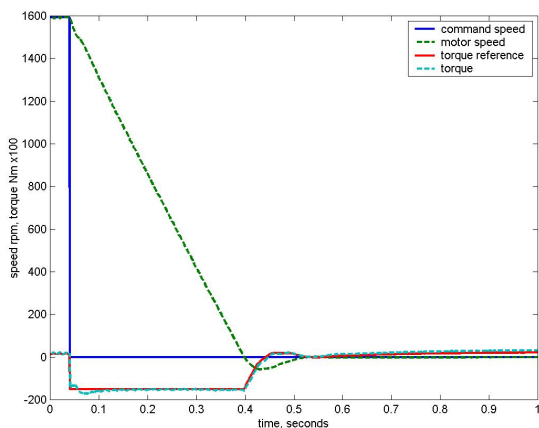


Figure 72: Step speed response. 1600 to 0 rpm, torque limit set to 1.5 Nm.

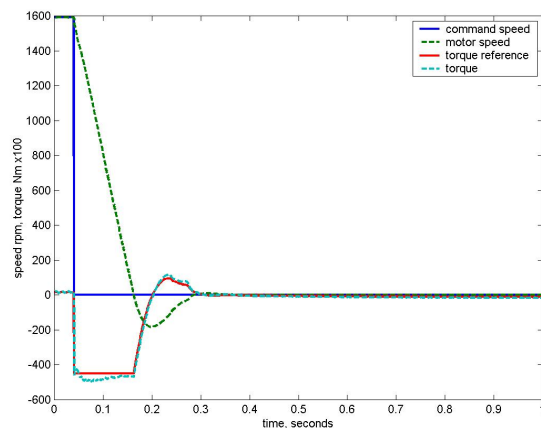


Figure 73: Step speed response. 1600 to 0 rpm, torque limit set to 4.5 Nm.

Step Speed Reversal

Figures 74 and 75 show the response to step speed reversals again a torque limits settings of 1.5 and 4.5 Newton-meters.. Again, speed and torque are very well behaved with no limitations at zero speed.

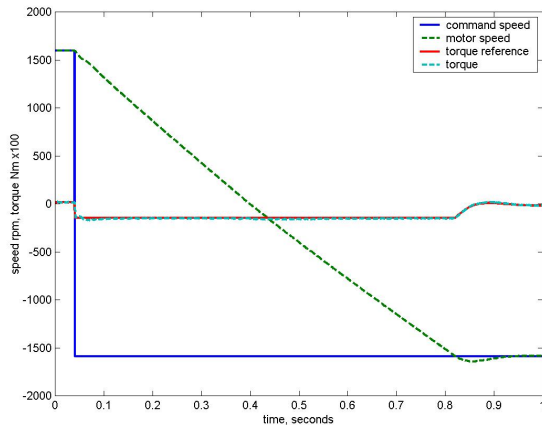


Figure 74: Speed reversal response, torque limit set to 1.5 Nm.

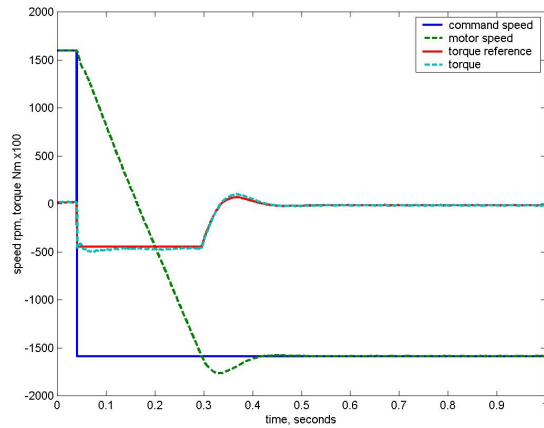


Figure 75: Speed reversal response, torque limit set to 4.5 Nm.

Step Load Response

Figure 76 shows the controller's response to a step change in load, in this instance from 4 Newton-meters to zero. The response time is mainly limited by the bandwidth of the outer speed loop.

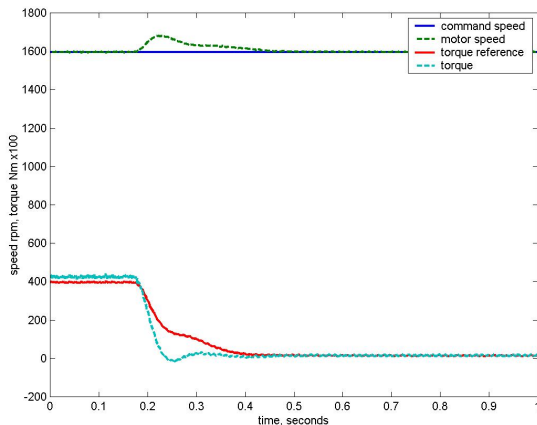


Figure 76: Step load torque response, 4 to 0 Nm.

Overload Response

Figures 72 and 71 show the results of imposing a torque overload sufficient to stall the motor. A load torque of 4 Nm is applied with the controller's torque limit set to only 2 Nm. The Magtrol dynamometer is set up to supply a fixed load torque of 4 Nm down to zero speed but not at zero speed, resulting in the motor stalling at zero speed. A limitation of the controller is that it cannot synchronise with a stalled motor. As a result, as shown in Figure 72, the controller's speed output expressed as the frequency of rotation of the applied motor current rises to a few rpm, but the actual motor is stalled and synchronism with the controller is lost. In this situation, the torque as shown is

not the motor torque but only a measure of the motor current. All the controller can do is to limit the motor current and keep its output frequency and thus the applied speed to a low level. As seen in Figure 71, once the overload is removed, the controller immediately synchronises with the rotor position and the motor accelerates under controlled torque to the set speed.

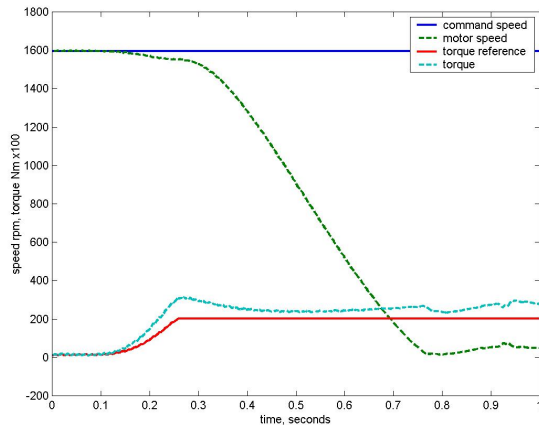


Figure 77: Overload response: 4 Nm load applied with a 2 Nm torque limit setting.

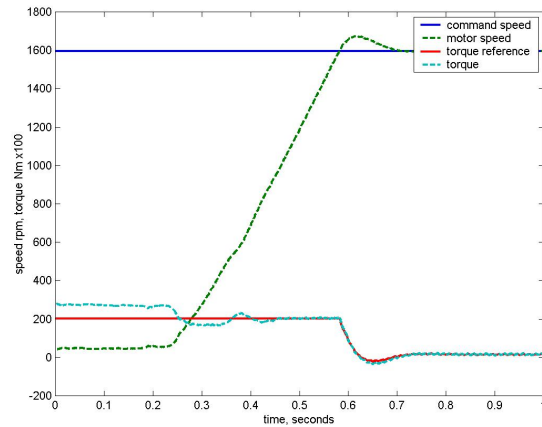


Figure 78: Recovery from overload: 4 Nm load removed with a 2 Nm torque limit setting.

References

1. P. Vas, *Sensorless Vector and Direct Torque Control*, New York.: Oxford University Press, 1998.
2. P. P. Acarnley and J. F. Watson. "Review of position-sensorless operation of brushless permanent-magnet machines," *IEEE Trans. Ind. Electron.*, vol. 53, no. 2, pp. 352-362, Apr. 2008.
3. M. Schroedl. "Sensorless control of AC machines at low speed and standstill based on the "INFORM" method," in *Conf. Rec. IEEE-IAS Annu. Meeting*, vol. 1, 1996, pp. 270-277.
4. E. Robeischl and M. Schroedl. "Optimized inform measurement sequence for sensorless PM synchronous motor drives with respect to minimum current distortion," *IEEE Trans. Ind. Applicat.*, vol. 40, pp. 591-598, Mar./Apr. 2004.
5. S. Shinnaka. "A new speed-varying ellipse voltage injection method for sensorless drive of permanent-magnet synchronous motors with pole saliency—new PLL method using high-frequency current component multiplied signal," *IEEE Trans. Ind. Applicat.*, vol. 44, pp. 777-788, May/June 2008.
6. R. S. Colby and D. W. Novotny. "An efficiency-optimising permanent-magnet synchronous motor drive," *IEEE Trans. Ind. Appl.*, vol. 24, no. 3, pp. 462-469, May/June 1988.
7. J. Itoh, N. Nomura and H. Osawa. "A comparison between v/f control and position-sensorless vector control for the permanent magnet sensorless motor," *Proc. Power Conversion Conf.*, 2002, vol.3, pp. 1310-1315, April 2002.
8. P. Acarnley, *Stepping Motors: a guide to theory and practice*, 4th ed. Stevenage, U.K.: Inst. Elect. Eng., 2002.
9. B. Bae, S. Sul, J. Kwon and J. Byeon. "Implementation of sensorless vector control for

- super-high-speed PMSM of turbo-compressor," *IEEE Trans. Ind. Appl.*, vol. 39, no. 3, pp. 811-818, May/June 2003.
10. Y. Iwaji, T. Sukegawa, T. Okuyama, T. Ikimi, M. Shigyo and M. Tobise. "A new PWM method to reduce beat phenomenon in large-capacity inverters with low switching frequency," *IEEE Trans. Ind. Appl.*, vol. 35, no. 3, pp. 606-612, May/June 1999.
 11. S. R. Bowes and Y. Lai. "The relationship between space-vector modulation and regular-sampled PWM," *IEEE Trans. Ind. Electron.*, vol. 44, no. 5, pp. 670-679, Oct. 1997.
 12. A. M. Hava, R. J. Kerkman and T. A. Lipo. "Simple analytical and graphical methods for carrier-based PWM-VSI drives," *IEEE Trans. Power Electron.*, vol. 14, no. 1, pp. 49-61, Jan. 1999.
 13. K. W. Tsui, N. C. Cheung and K. C. Yuen. "Novel modeling and damping technique for hybrid stepper motor," *IEEE Trans. Ind. Electron.*, vol. 56, no. 1, pp. 202-211, Jan. 2009.
 14. S. Yang and E. Kuo. "Damping a hybrid stepping motor with estimated position and velocity," *IEEE Trans. Power Electron.*, vol. 18, no. 3, pp. 880-887, May 2003.
 15. K. Y. Cho, S. B. Yang and C. H. Hong. "Sensorless control of a PM synchronous motor for direct drive washer without rotor position sensors," *IEE Proc. Electr. Power Appl.*, vol. 151, no. 1, pp. 61-69, Jan. 2004.
 16. Y. Murai, T. Watanabe and H. Iwasaki. "Waveform distortion and correction circuit for PWM inverters with switching lag-times," *IEEE Trans. Ind. Appl.*, vol. 23, no. 5, pp. 881-886, Sept./Oct. 1987.
 17. S. Jeong and M. Park. "The analysis and compensation of dead-time effects in PWM inverters," *IEEE Trans. Ind. Electron.*, vol. 38, no. 2, pp. 108-114, April 1991.
 18. D. Leggate and R. J. Kerkman. "Pulse-based dead-time compensator for PWM voltage inverters," *IEEE Trans. Ind. Electron.*, vol. 44, no. 2, pp. 191-197, April 1997.
 19. K. J. Åström and L. Rundqwist. "Integrator windup and how to avoid it," *American Control Conf.*, 1989, pp. 1693-1698, 21-23 June 1989.
 20. G. Ellis and R. D. Lorenz. "Comparison of motion control loops for industrial applications," *Proc. IEEE IAS Annu. Meeting*, Phoenix, AZ, 1999, vol. 4, pp. 2599-2605.
 21. D. Kaiser, "Fundamentals of servo motion control," Parker Hannifin Compumotor Division, Technical Notes, 1997.
 22. S. Chi, Z. Zhang and L. Zhu. "Sliding-mode sensorless control of direct-drive PM synchronous motors for washing machine applications," *IEEE Trans. Ind. Appl.*, vol. 45, no. 2, pp. 582-590, Mar./Apr. 2009.